CONF-900289--4

DE90 009809

NEGATIVE ION FORMATION PROCESSES: A GENERAL REVIEW

G. D. ALTON
Oak Ridge National Laboratory,* P. O. Box 2008, Oak Ridge, Tennessee 37831-6368

Abstract The principal negative ion formation processes will be briefly reviewed. Primary emphasis will be placed on the more efficient and universal processes of charge transfer and secondary ion formation through non-thermodynamic surface ionization.

INTRODUCTION

The existence of the negative ion state has provided us with an additional means for producing charged beams containing most of the naturally occurring chemically active elements. Negative ion beams have been used for many years in high-energy, accelerator-based atomic, nuclear, and applied research, as well as low-energy fundamental atomic physics and controlled thermonuclear research programs. Negative ions are also being utilized in a variety of applied research, including tandem accelerator-based high-energy ion implantation, radiation damage, high-energy sputtering, and in surface analysis based on Rutherford backscattering spectrometry (RBS), secondary ion mass spectrometry (SIMS), tandem accelerator mass spectrometry (TAMS), x-ray fluorescence, and hydrogen depth profiling. Important to the theme of this conference is the fact that negative ion beams of H^- play an important role in Lamb shift,[1] optically pumped,[2-4] and atomic beam[5] ion sources for the production of intense, nuclear spin polarized proton beams for use in high-energy spin physics experiments. These and other negative ion applications have provided the impetus for the development of sources capable of producing negative ion beams containing almost every element in the periodic chart.[6,7]

* Research sponsored by the U.S. Department of Energy under contract DE-AC05-84OR21400 with Martin Marietta Energy Systems, Inc.

"The submitted manuscript has been authored by a contractor of the U.S. Government under contract No. DE-AC05-84OR21400. Accordingly, the U.S. Government retains a nonexclusive, royalty-free license to publish or reproduce the published form of this contribution, or allow others to do so, for U.S. Government purposes."

MASTER

DISTRIBUTION OF THIS DOCUMENT IS UNLIMITED

In this review, brief descriptions are given of the negative ion formation processes of radiative capture, dielectronic attachment, polar disassociation, dissociative attachment, tenerary collisional attachment, charge transfer, and thermodynamic and non-thermodynamic equilibrium surface ionization. Particular emphasis will be placed on parameters important for generating negative ion beams by the more universal and high probability processes of charge transfer and secondary ion formation through non-thermodynamic surface ionization. In addition, the electron affinities of the elements are reviewed and a limited amount of electron affinity data are provided. For more detailed information concerning negative ions, negative ion sources, and methods of negative ion formation, the reader is referred to reviews such as those by Massey[8] and Smirnov[9] and to references cited within the present report.

THE NEGATIVE ION STATE

The Electron Affinity

The processes involved in the attachment of electrons to neutral atoms or molecules are exothermic in contrast to the endothermic processes required for positive ion formation. The parameter which characterizes the negative ion is the binding energy of the additionally attached electron or electron affinity E_A. The binding energy or electron affinity E_A of the negative ion is a measure of the stability and ease of ion formation, as well as ease of detachment. The electron affinity E_A is defined as the difference in energies of the neutral atom E_0 and negative ion states E_- given by

$$E_A = E_0 - E_- . \tag{1}$$

E_A must be positive for stable or metastable negative ion formation.

The Electron Affinities of the Elements

Approximately 78% of the naturally occurring elements have positive electron affinities. Table I displays experimentally determined atomic electron affinities for many of the naturally occurring elements – many of which were taken from the compilations of Ref. 10. The electron affinities of the elements have values ranging from $E_A \leq 0$ to E_A = 3.618 eV for Cl. We note that Be and Mg of the group IIA elements and all members of the group IIB and VIIIA elements, as well as the elements N, Sc, Mn, Y, and Hf, have negative ground state electron affinities.

Table I A partial list of the ionization potentials and electron affinities of the naturally occurring elements.

(Key: element; IONIZATION POTENTIAL; ELECTRON AFFINITY)

GROUP IA	IIA	IIIA	IVA	VA	VIA	VIIA	VIII A
1 H 13.595 0.7542							2 He 24.58 0.078*
3 Li 5.39 0.620	4 Be 9.32 0.19*	5 B 8.30 0.28	6 C 11.26 1.268	7 N 14.54 <0	8 O 13.61 1.462	9 F 17.42 3.399	10 Ne 21.56 <0
11 Na 5.14 0.548	12 Mg 7.64 <0	13 Al 5.98 0.46	14 Si 8.15 1.385	15 P 10.55 0.743	16 S 10.36 2.0772	17 Cl 13.01 3.615	18 Ar 15.76 <0
19 K 4.34 0.5012	20 Ca 6.11 0.043	31 Ga 6.00 0.3	32 Ge 7.88 1.2	33 As 9.81 0.80	34 Se 9.75 2.0206	35 Br 11.84 3.364	36 Kr 14.00 <0
37 Rb 4.18 0.4860	38 Sr 5.69 >0	49 In 5.78 0.3	50 Sn 7.34 1.25	51 Sb 8.64 1.05	52 Te 9.01 1.9708	53 I 10.45 3.061	54 Xe 12.13 <0
55 Cs 3.89 0.4715	56 Ba 5.21 >0	81 Tl 6.11 0.3	82 Pb 7.41 0.36	83 Bi 7.29 1.1	84 Po 8.43 1.9	85 At 9.5 2.8	86 Rn 10.74 <0

III B	IV B	V B	VI B	VII B	VIII B			I B	II B
21 Sc 6.56 <0	22 Ti 6.83 0.2	23 V 6.74 0.5	24 Cr 6.76 0.66	25 Mn 7.43 <0	26 Fe 7.90 0.25	27 Co 7.86 0.7	28 Ni 7.63 1.15	29 Cu 7.72 1.226	30 Zn 9.39 <0
39 Y 6.5 =0	40 Zr 6.95 0.5	41 Nb 6.77 1.0	42 Mo 7.18 1.0	43 Tc 7.28 0.7	44 Ru 7.36 1.1	45 Rh 7.46 1.2	46 Pd 8.33 0.6	47 Ag 7.57 1.303	48 Cd 8.99 <0
57 La 5.61 0.5	72 Hf 7. <0	73 Ta 7.88 0.6	74 W 7.98 0.6	75 Re 7.87 0.15	76 Os 8.7 1.1	77 Ir 9. 1.6	78 Pt 8.96 2.128	79 Au 9.22 2.3086	80 Hg 10.43 <0

*METASTABLE

The group IIA elements span the complete spectrum of possible electron affinities. Be has a negative ground state electron affinity, but is bound metastably in the $1s^2 2s2p^2(^4P)$ state; the ion is metastable against direct Coulomb autodetachment and electric dipole radiative decay processes, has a lifetime of a few μ s, and thus lives long enough for practical use.[11] Mg, on the other hand, forms neither a bound ground state nor metastably bound state and thus cannot be produced as an atomic negative ion. On the other hand, the heavier members of the group (Ca, Sr and Ba) all form or are believed to form stably bound ground state negative ions. For example, Ca^- is bound in the [Ar] $s^2p(^2P)$ electronic configuration by 45 meV.[12] While the electron affinities of Sr and Ba have not been measured to date, they are expected to be stably bound in the [Kr] $s^2p(^2P)$ and [Xe] $s^2p(^2P)$ states, respectively, similar to Ca^-.[13]

In addition to negative atomic species, many molecular negative ions have been observed. In many cases, molecular negative ions containing the atom of interest have much higher electron affinities than the atom itself and, therefore, can be formed with higher probability than can the atomic species. In some cases, molecular ions offer the only alternative for producing beams containing elements which do not form stably bound negative ion states. For tandem accelerator applications, the unwanted species can be easily rejected by collisional dissociation in the positive ion formation process (stripping) followed by magnetic (m/q) analysis. Table II provides a partial list of electron affinities of molecular species containing elements which have negative or low positive electron affinities. These data were derived from Refs. 14-25.

TABLE II A list of electron affinities for a few molecules.

Molecular Radical	E_A (eV)	Reference
BO	2.79	14
BO_2	4.1	15
BeO	1.76	16
CN	3.82	17
FeO	1.49	18
LiH	0.4	19
LiN	0.4	19
NaH	0.32	19
NH	0.38	20
NH_2	0.76	21
N_2O	0.22	22
NO_2	3.1	23
UF_6	4.9	24
WF_6	4.3	25

Metastable Negative Ion Formation

There is an important class of negative ions which can be formed in excited states of the parent atom and live long enough to be of use experimentally. Such long-lived states are categorized as being metastable. In order to induce electron attachment and thus form such states, it is necessary, first of all, to form a particular excited electronic state of the neutral atom to which an electron can be attached. The charge

transfer process which will be discussed later in this report is particularly well suited for metastable ion formation. The subsequently formed negative ion may live for extended periods of time if decay of the excited compound state is forbidden.

Classic examples of metastable negative ions which can only be formed through attachment to excited states of the parent atoms are He^-,[26,27] and Be^-,[11]. He^- and Be^- form with high probabilities in the ^4P states through sequential charge exchange with a low ionization potential charge exchange vapor M such as a member of the group IA elements through the following spin conserving interactions:

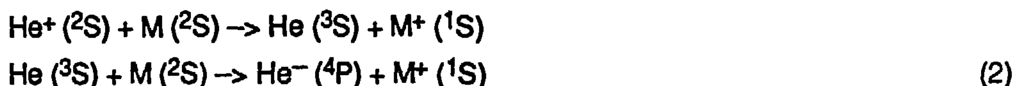

$$He^+ (^2S) + M (^2S) \rightarrow He (^3S) + M^+ (^1S)$$
$$He (^3S) + M (^2S) \rightarrow He^- (^4P) + M^+ (^1S) \quad (2)$$

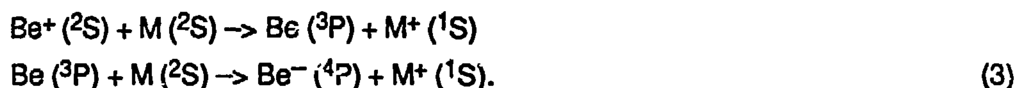

$$Be^+ (^2S) + M (^2S) \rightarrow Be (^3P) + M^+ (^1S)$$
$$Be (^3P) + M (^2S) \rightarrow Be^- (^4P) + M^+ (^1S). \quad (3)$$

The attachment energy for He^- relative to the He (^3S) state is 78 meV and is metastable against direct Coulomb autodetachment and electric dipole radiative decay processes.[26,27] The lifetime of the negative ion depends on the particular magnetic substate; the $P_{1/2,3/2}$ states have lifetimes of ~10 and 16 μs, respectively, and the $P_{5/2}$ substate has a much longer lifetime (~500 μs).[28,29] Be^- is also formed in the ^4P state which lives for a few μs before autodetaching.[11] Evidence of the metastability of Be^- is displayed in Fig. 1 which shows the electron energy spectrum of the autodetaching ^4P state.

The He_2^- molecular ion is a very interesting example of a spin-aligned, complex negative ion state. Two distinct autodetachment channels are observed in the electron energy spectra of He_2^- formed by sequential charge transfer of energetic He_2^- in lithium vapor.[30] A single narrow peak is observed which is attributed to vibrational autodetachment, e.g., $He_2^-\left(^4\Pi_g\right)_{v=1} \rightarrow He_2^0\left(a^3\Sigma_u^+\right)_{v=0} + e$). The second peak is broad and results from autodetachment of He_2^- into the $He_2(X^1\Sigma_g^+) + e$ repulsive continuum. The electron affinity for the $^4He_2(a^3\Sigma_u^+)$ state is found to be 0.175 eV, while that for the analogous $^3He_2\left(a^3\Sigma_u^+\right)$ state is 0.178 eV.

Fig. 1. Electron energy spectra from 55 keV Be^- ions with and without a thin argon target illustrating the metastable nature of the ion species (Ref. 11).

PRINCIPAL NEGATIVE ION FORMATION PROCESSES

Negative Ion Formation Through Electron Impact or Photo-dissociation

Radiative Capture The simplest way in which negative ions can be formed is by direct capture of a free electron by a neutral atom according to the following interaction:

$$e + X \rightarrow X^- + h\nu. \qquad (4)$$

For attachment to take place, the initial kinetic energy of the electron T_e plus the electron affinity E_A must be released through radiation or transfer to a third body. Such mechanisms are referred to as radiative capture processes and are characterized by a continuum emission of radiation with longest wavelength given by

$$\lambda = \frac{hc}{E_A} \tag{5}$$

whenever third body energy transfer processes are not involved. The process, however, occurs with low probability and, therefore, is not a practical means of producing negative ions.

Dielectronic Attachment Another attachment mechanism is possible involving radiative stabilization. Attachment is possible if the incident electron has energy such that the energy of the atom plus electron is within the level width of a doubly excited state of the atom. Thus, it is possible to capture the electron by reverting to the ground state by radiative emission; the atom may revert back to the neutral by ejecting the electron back into the continuum. Dielectronic attachment is a low probability process and, therefore, not important in high-intensity negative ion sources. The process for capture can be represented by the following interaction:

$$e + X \rightarrow X^- + h\upsilon. \tag{6}$$

Polar Dissociation Attachment may occur as a result of photon,electron, or heavy particle interactions with molecular neutrals in which sufficient energy is imparted to the molecule to excite the molecule to an unstable state which dissociates spontaneously into positive and negative ions.

Polar photodissociative attachment is a process whereby a molecule XY absorbs a photon of sufficient energy $h\upsilon$ to cause spontaneous fragmentation according to the reaction

$$XY + h\upsilon \rightarrow X^- + Y^+. \tag{7}$$

Negative ion formation may also occur by this mechanism, as well, whenever an electron of sufficient energy for molecular excitation to an unstable state interacts with a molecule XY as follows

$$e + XY \rightarrow X^+ + Y^- + e. \tag{8}$$

We note that the electron is not itself captured, but only serves as the means by which the molecular excitation occurs.

In polar dissociation processes, the Franck-Condon principle can be invoked to estimate the relative kinetic energy of the X^+ and Y^- ions after the collision.[31,32] If the minimum energy transfer necessary for molecular fragmentation to occur is given by E_{min} and the dissociation energy D_{XY} is known along with the ionization energies of the positive and negative ion fragments E_I, E_A respectively, the minimum relative kinetic energy T of the fragments can be calculated from the following expression:

$$T = E_{min} + E_A - E_i - D_{XY}. \tag{9}$$

Dissociative Attachment Electrons may be stably attached to atoms during their interactions with molecular neutrals according to the following reactions:

$$e + XY \rightarrow X^- + Y$$
$$e + XY \rightarrow X + Y^-. \tag{10}$$

The process may be viewed as a three-body process where the excess energy released during the reaction can be adsorbed by transfer to the relative motion of the atomic nuclei or fragments and thus the state can be readily stabilized. Such processes are characterized by curve crossing of the respective molecular-neutral and negative-neutral potential energy curves as illustrated in Fig. 2.

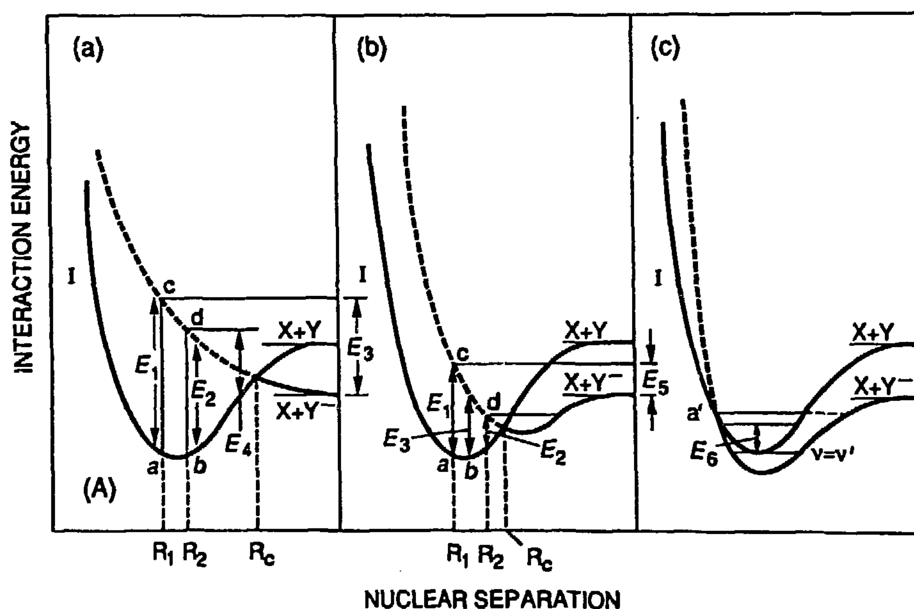

Fig. 2. Potential energy curves illustrating three possible ways for electron attachment to a molecule XY or dissociative attachment to one of the fragments.

In Figs. 2a, b, and c, the solid curves refer to the ground or normal states of the neutral molecule XY; the dotted curves refer to states of the molecular negative ion. In the limit toward infinite nuclear separation, the curves are spread apart by an amount equal to the electron affinity of the atom Y. The range of nuclear separations $R_1 \rightarrow R_2$ corresponds to the amplitude of oscillation (a -> b) of the molecule in the ground or normal state. The transition resulting in electron capture will occur between points c and d, provided that the nuclear coordinates R_1 and R_2 remain fixed (Franck-Condon principle). Autodetachment can occur over a considerable range of nuclear separations. Molecules which survive without autodetachment will dissociate into an atom X and an ion Y^- with relative kinetic energy between E_3 and E_4. Once the nuclear separation R passes R_c, autodetachment can no longer take place (Fig. 2a).

In Fig. 2b, electrons captured with energy between E_3 and E_1 can produce dissociative attachment of atoms X and ions Y^- with relative energies between 0 and E_5. Electrons which are captured with energies between E_2 and E_3 induce vibrational excitation of the molecule XY^-.

Attachment to the molecule can occur for molecules with positive electron affinities without dissociation, thereby forming the molecule XY^-. Vibrational states of the molecule will be stable for frequencies $\upsilon < \upsilon'$; those with vibrational frequencies $\upsilon > \upsilon'$ will be unstable toward autodetachment (Fig. 2c). Again, this process is possible because electronic excitations take place on a time scale short with respect to the motion of nuclei (Franck-Condon principle).

<u>Production through Ternary Collisions between Electrons and Molecules</u> Ternary collisions are the most efficient in producing negative ions in a dense gas or plasma at low electron energies. These occur as follows:

$$\begin{aligned} &e + X + Y \rightarrow X^- + Y \\ &X + 2e \rightarrow X^- + e \end{aligned} \qquad (11)$$

where X and Y are atoms or molecules, and e is the electron. The first process is of much greater practical importance because the second occurs only in systems with high electron densities.

While all of the previously discussed radiative and collisional processes may take place in certain types of negative ion sources, radiative and dielectronic capture are known to be low probability processes and, therefore, are not practical mechanisms for negative ion production. In most sources, utilizing charged particles for production (electrons or ions), photo-polar dissociation processes are infrequent because of the low photon flux environment. In direct-extraction plasma-type negative

ion sources, electron polar dissociation, dissociative attachment, and three-body (ternary) collisional transfer processes dominate.

The reader is referred to Refs. 6 and 7 for a review of direct extraction plasma-type negative ion sources for the production of heavy negative ions, and to Ref. 33 for a review of volume-type H^- ion sources.

Negative Ion Formation through Charge Transfer

The single charge transfer process is often referred to as "charge exchange" or "electron capture." The charge transfer process can be represented by the following projectile X target Y interaction where ΔE is referred to as the energy defect:

$$X^+ + Y \rightarrow X + Y^+ + \Delta E. \qquad (12)$$

In general, the collision takes place at relatively large impact parameters, for which the projectile scattering angle is small and the product ion is scattered nearly perpendicular to the impact momentum vector. From the standpoint of beam quality degradation, low-momentum transfer pressures are clearly desirable.

Such transfer processes can be cast into two distinct categories: (1) symmetrical (resonance) processes, and (2) unsymmetrical or non-resonance processes. In the first category, the projectile and target are the same species while in the latter category, which is of generally of more practical importance as a means of producing negative ion beams, the projectile and target are different.

Symmetrical (Resonance) Charge Transfer

The symmetrical charge transfer process in which the projectile and target are identical can be described by the following reaction:

$$X^+ + X \rightarrow X + X^+ + \Delta E. \qquad (13)$$

The energy defect is equal to the difference between the ionization energies, i.e., $\Delta E = E_i(X) - E_i(X)$ and is, thus, zero. Hence, the cross sections can be very large. Negative ion formation requires the following sequential projectile-target reactions:

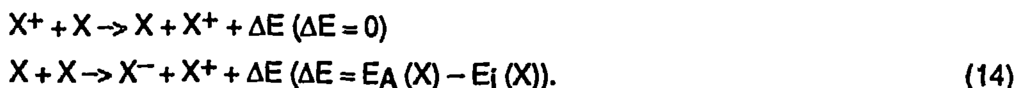

$$X^+ + X \rightarrow X + X^+ + \Delta E \; (\Delta E = 0)$$
$$X + X \rightarrow X^- + X^+ + \Delta E \; (\Delta E = E_A(X) - E_i(X)). \qquad (14)$$

As noted, the energy defect for the second reaction is equal to the difference between the electron affinity of the first projectile atom E_A and the ionization energy E_i of the stationary target atom. Thus, symmetrical processes may not necessarily be

commensurate with efficient negative ion formation because of the possibility of a high ionization energy E_i for the donor species. However, consideration may be given to a two-step process in which the first process is symmetrical, for which the cross section is large for neutral energetic atom formation, followed by an asymmetrical non-resonance process in which the energy defect is much smaller, e.g.,

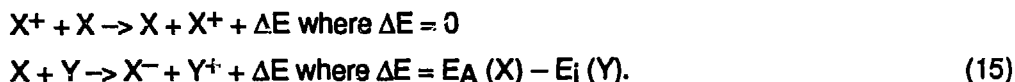

$$X^+ + X \rightarrow X + X^+ + \Delta E \text{ where } \Delta E = 0$$
$$X + Y \rightarrow X^- + Y^+ + \Delta E \text{ where } \Delta E = E_A(X) - E_i(Y). \quad (15)$$

Obviously, the energy defect can be minimized by selection of a charge transfer medium which has a low first ionization energy E_i (Y). Cesium is an excellent choice because it has the lowest ionization energy of the elements.

Theoretical Description The cross section for the symmetrical charge transfer process has been shown to decrease with projectile velocity v according to

$$\sigma^{1/2} = a - b\ln(v) \quad (16)$$

when a and b are constants. The cross section given by the usual expression

$$\sigma = 2\pi \int_0^{\infty} b\, P(b)\, db \quad (17)$$

where b is the impact parameter and P(b) is the probability of finding the system in the final state of interest. For an ion moving along the x direction and interacting with a target atom at impact parameter b with respect to the direction of projectile motion, the probability is given by[34]

$$P(b,\vec{v}) = \sin^2\left\{\int_{-\infty}^{\infty} \frac{E_i\left(x^2+b^2\right)^{1/2}}{\hbar v a_o} \exp\left[-\left(\frac{E_i}{13.6}\right)^{1/2} \frac{\left(x^2+b^2\right)^{1/2}}{a_o}\right] dx\right\} \quad (18)$$

where a_o is the first Bohr orbital. The cross section, thus, is oscillatory in impact parameter b. Measured symmetrical charge transfer cross sections[35] for $H^+ + H$ versus projectile energy E are compared with the calculations of Ref. 36 in Fig. 3.

Asymmetrical (Non-Resonant) Charge Transfer

The most general application of the charge exchange formation technique is for interactions between unlike ions. These processes occur with high probability between projectiles interacting with exchange vapors which possess a low energy

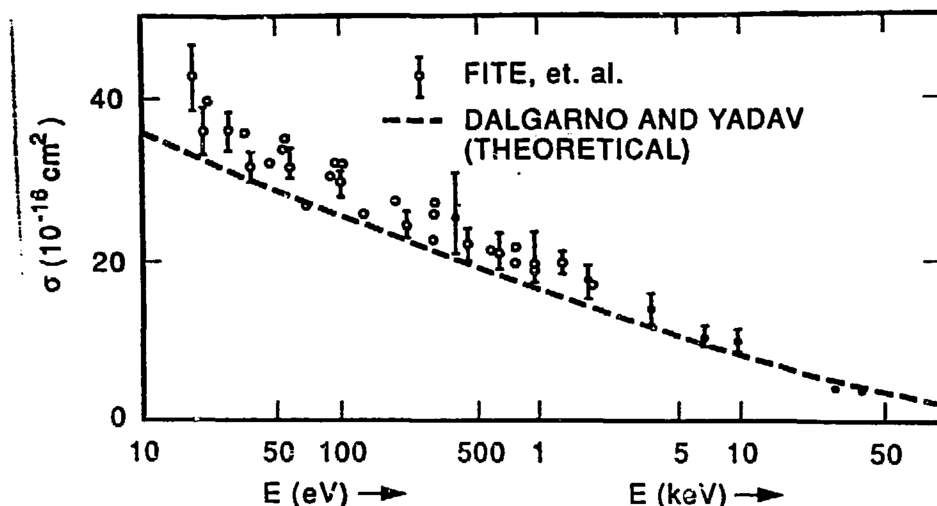

Fig. 3. Symmetrical (resonance) single-electron charge transfer cross section σ versus H^+ Energy E in hydrogen. (o experimental (Ref. 35); ..... theoretical (Ref. 36)).

defect. The probability for charge transfer from the electron donor (exchange vapor) and the projectile ion is sensitively dependent on the velocity of the projectile.

The atomic charge transfer process occurs between unlike ions and differs from the symmetric resonance process in that it involves an electronic transition which requires a change in internal energy of the system referred to as the energy defect ΔE. The energy defect ΔE of the process

$$X^+ + Y \rightarrow X + Y^+ + \Delta E \qquad (19)$$

can be equated to the difference between the ionization energies E_i of the interacting atoms or molecules as

$$\Delta E = E\,(X^+) - E\,(X) + E\,(Y) - E\,(Y^+) = E_i\,(X) - E_i\,(Y). \qquad (20)$$

Two-electron capture during a single collision is much less likely due to the very high energy defect as seen from the following reactions:

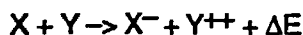

$$X + Y \rightarrow X^- + Y^{++} + \Delta E$$

where $\Delta E = E_A\,(X) - E_i\,(Y) - E_i\,(Y^+)$. (21)

Rapp and Francis[34] derived the following expression which relates the cross section for non-resonance electron transfer σ and impact parameter b:

$$\sigma = \int_0^{\infty} \operatorname{sech}^2\left[\frac{|\Delta E|}{hv}\left\{\left(\frac{13.6}{E_i}\right)^{1/2}\frac{\hbar^2\pi b}{2m_e e^2}\right\}^{1/2}\right]2\pi b db. \tag{22}$$

In expression 22, ΔE is the energy deficit, E_i is the ionization energy of the projectile of velocity v, and m_e is the mass of the electron. Comparisons are made between Eq. 22 and the experimental data of Ref. 37 for resonant and non-resonant interactions involving H^+ interacting with H and He, Ne and Ar and with exchange media with energy defects $\Delta E = 1,3,5$ and 10 eV in Fig. 4.

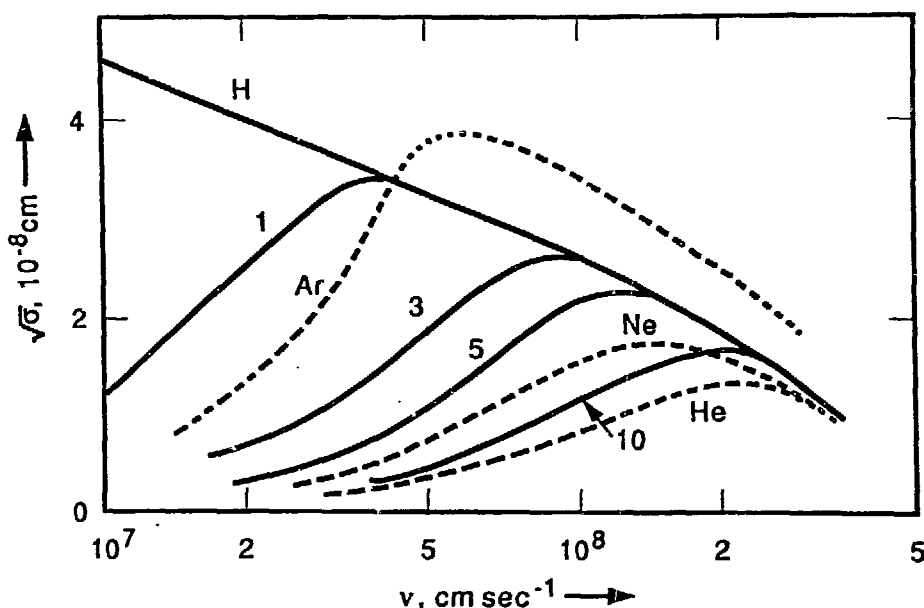

Fig. 4. Comparison of theoretical and experimental symmetrical (H^+ on H) and asymmetrical charge transfer cross sections (H^+ on He, Ne, and Ar) and for $\Delta E = 1, 3, 5$, and 10 eV versus H^+ velocity. —— theoretical (Ref. 34); - - - experimental (Ref. 37).

The formation of metastable H (^2S) is of fundamental importance in Lamb-shift spin polarized sources[1] and several studies of the cross sections for electron capture in various noble gases, H_2 and alkaline and alkaline earth metal vapors have been made, including those described in Refs. 38 through 43. These studies usually involve quenching the H(^2S) state in a high-electric field. Examples of single electron capture for energetic H^+ in He, Ar, Mg, and Ba vapors[43] are shown in Fig. 5. These data illustrate clearly the advantage of an alkaline-earth metal charge transfer media over noble gases. Single and double electron transfer cross sections for H^+ projectiles versus projectile energy E interacting with various group IIA element vapors[43,44] are contrasted in Figs. 6 and 7, respectively. The cross-sections are small at the lowest energies, rise to a maximum, and fall off at high energies as would be expected of the symmetrical resonance process.

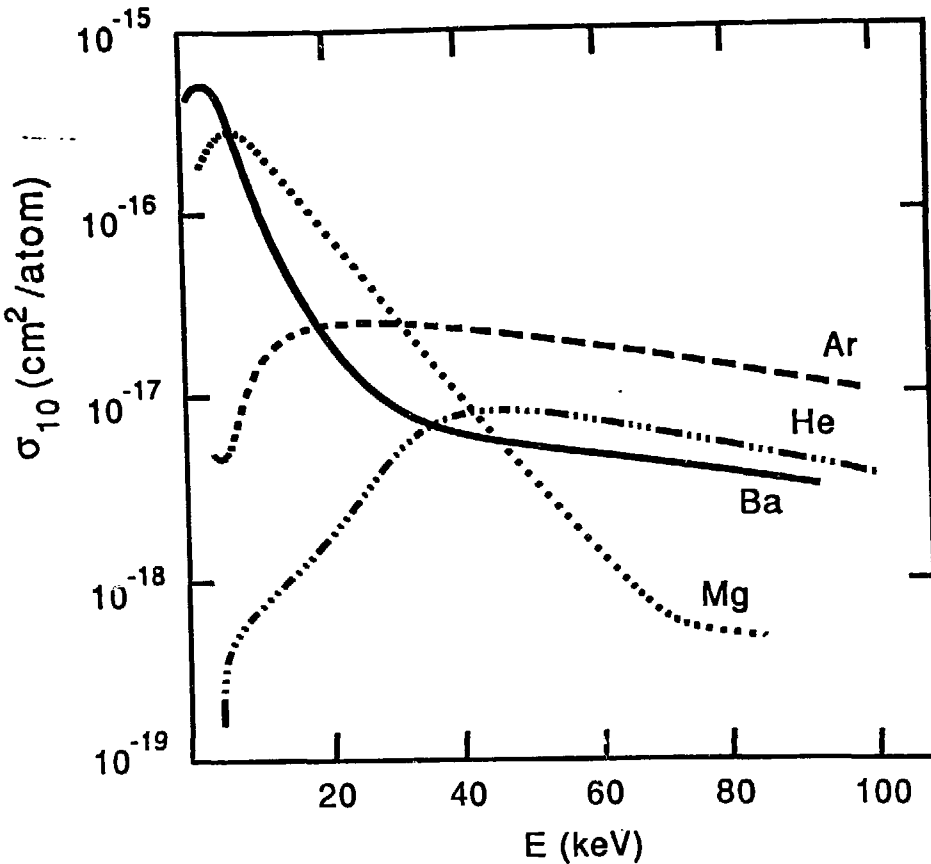

Fig. 5. Single electron capture σ_{10} into the H(^{2}S) state versus H+ energy E in He and Ar gases and Mg and Ba vapors (Ref. 43).

The Massey Adiabatic Criterion The adiabatic criterion proposed by Massey[45] is of practical importance in charge transfer collisions. At low projectile energies, where the relative motion of the atoms is slow enough so that electronic motion can adiabatically adjust to small changes in the internuclear distance, the electron transfer process becomes unlikely. However, if the impact energy falls outside this 'adiabatic region' and the electronic transition time is comparable to the collision time, the probability for electron transfer can be very high. The time of collision is taken as a/v, where v is the impact velocity and a is known as the 'adiabatic parameter,' the parameter a is of the same order as atomic dimensions within which the charge transfer transition becomes likely. The characteristic time for the electronic transition is given by h/ΔE, where ΔE is the energy defect. Thus, the condition

$$v \ll \frac{a|\Delta E|}{h} \tag{23}$$

characterizes the adiabatic velocity region and

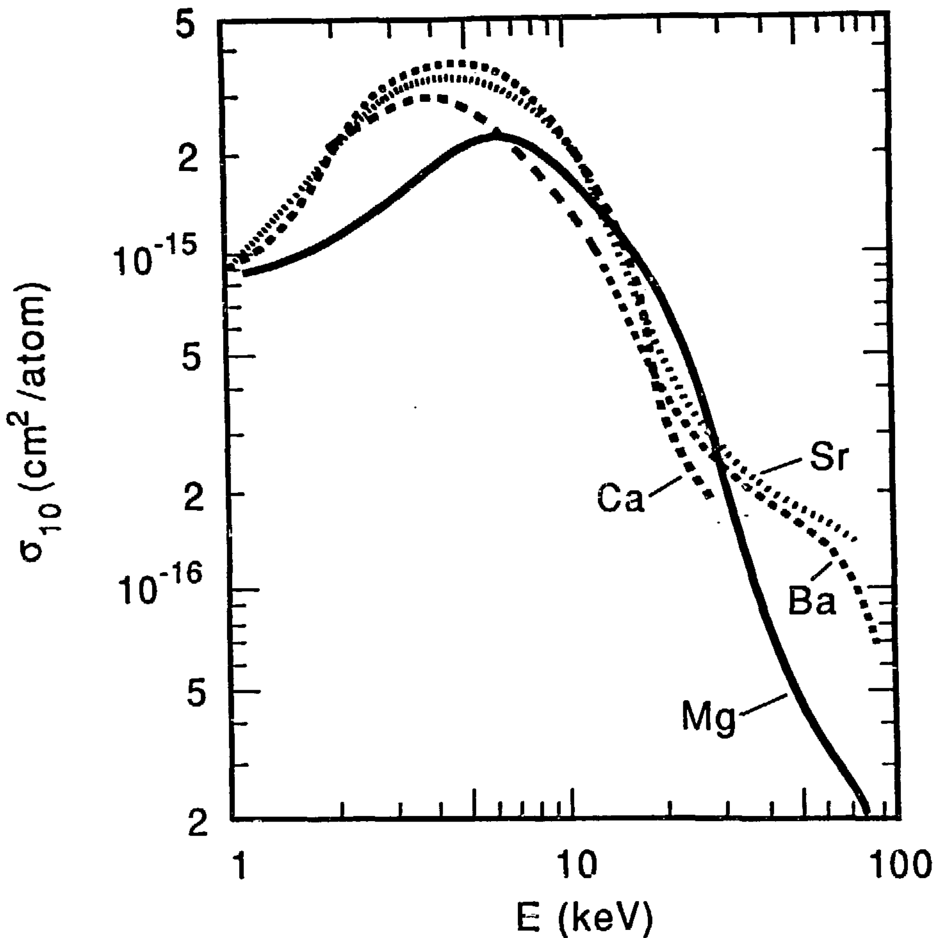

Fig. 6. Single electron capture cross sections σ_{10} versus H^+ energy E in various group IIA element vapors. (Mg and Ba: Ref. 43; Ca and Sr: Ref. 44).

$$v \cong \frac{a|\Delta E|}{h} \tag{24}$$

characterizes the velocity region for which the maximum in the charge transfer process occurs.

The criterion has been applied by Hasted to many charge transfer cross-section reactions at projectile energies E_{MAX} at which the cross sections have maximum values.[46] The assumption is made that the criterion holds as an equality at this energy. The energy E_{MAX} of a projectile of mass M_1 interacting with a stationary target then is given by

$$E_{MAX} = \frac{M_1}{2}\left(\frac{a\Delta E}{h}\right)^2. \tag{25}$$

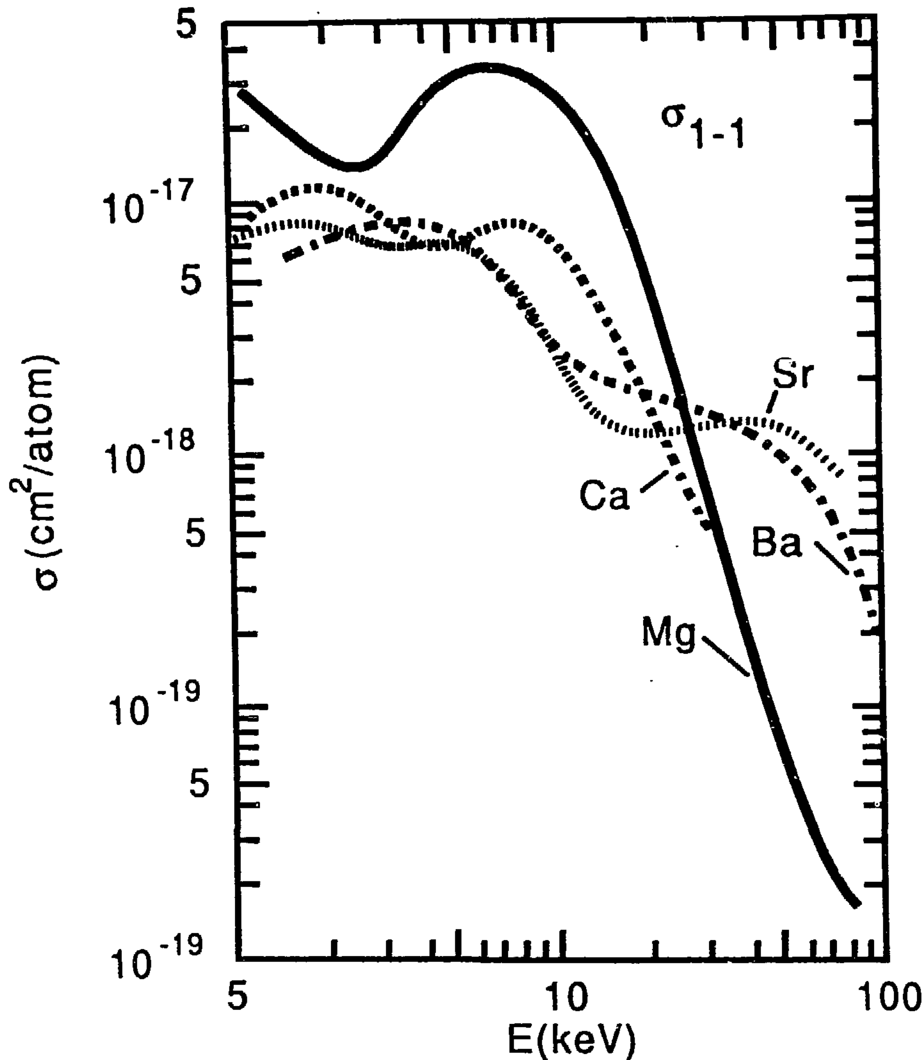

Fig. 7. Sequential two-electron capture cross sections $\sigma_{1\text{-}1}$ versus H^{+} energy E in various Group IIA element vapors: (Mg and Ba: Ref. 43, Ca and Sr: Ref. 44).

The parameter a, obtained from many different reaction processes, was found to have a value of a = 7 A^{0}. The "adiabatic maximum rule" is thus a convenient method of estimating the energy of a cross-section function maximum, apparently valid over a large range of impact energies.

Equilibrium Negative Ion Charge Transfer Fractions

The differential fraction of negative ions dFi produced during passage through a vaporous target of thickness dπ can be expressed in terms of a set of first order linear differential equations given by

$$dFi / d\pi = \Sigma F_j \sigma_{ji}, - \Sigma F_i \sigma_{ij} \quad (26)$$

where F_j, F_i are beam fractions in the jth and ith states, respectively, and σ_{ji}, σ_{ij} are cross sections for transferring electrons from state j to state i and from state i to state j. Solutions to the set of coupled equations requires the knowledge of n (n-1) cross sections for a system involving n states.

The electron capture and loss processes which take place during collisions between energetic ions and atoms or molecules in a gaseous vapor result in a statistical distribution of charge states of the emergent beam. Equilibrium between the competing capture and loss processes takes place whenever the beam passes through a target of sufficient thickness so that a balance between production and loss occurs. A particular emergent charge state is in equilibrium whenever the fraction no longer depends on further increases in target density. In order to efficiently generate negative ions by the charge transfer technique, knowledge of the dependence of the negative ion fraction F_{-1}^{∞} on cell temperature and ion energy is essential. Experimental schemes for measuring such processes have been described by several experimental groups, including the devices described in Refs. 38 and 47.

Equilibrium fractions F_{-1}^{∞} for H in several group IA, and group IIA metal vapor are shown in Fig. 8;[48] analogous equilibrium fractions for D in various group IA have also been measured in these vapors by this group.[48] An excellent review of charge transfer processes related to polarized ion sources is given in Ref. 49. Many other

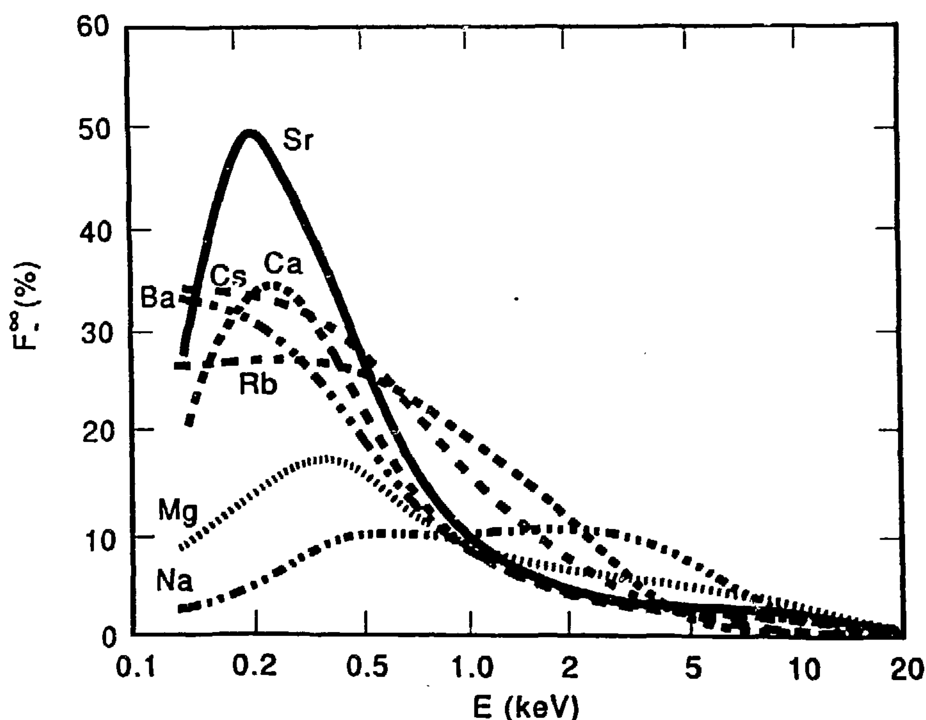

Fig. 8. Negative ion yields equilibrium yields F_{-}^{∞} as a function of H energy E in Sr, Ca, Cs, Ba, Rb, Mg, and Na vapors (Ref. 48).

investigations have been made of the probabilities and energy dependencies of charge transfer negative ion formation, including the following: H^- in Na,[50] and Cs vapors[51] and He^- in Li, Na and Mg,[52] K,[53] Rb,[54] and Cs[55] vapors.

Charge transfer, using both sodium and magnesium vapor, has also been utilized for the efficient production of many negative heavy ions during the past several years.[56,57] These investigations show production efficiencies ranging from ~0.5 to >90% for the elements considered. These studies show that Mg is a more effective electron donor for high electron affinity elements while Na vapor is desirable for the production of beams from low affinity materials. Further evidence of the efficiency and universal character of the charge transfer process is given in Figs. 9-12 for groups IA, IIIA, IVA, and VA projectiles in cesium vapor.[58]

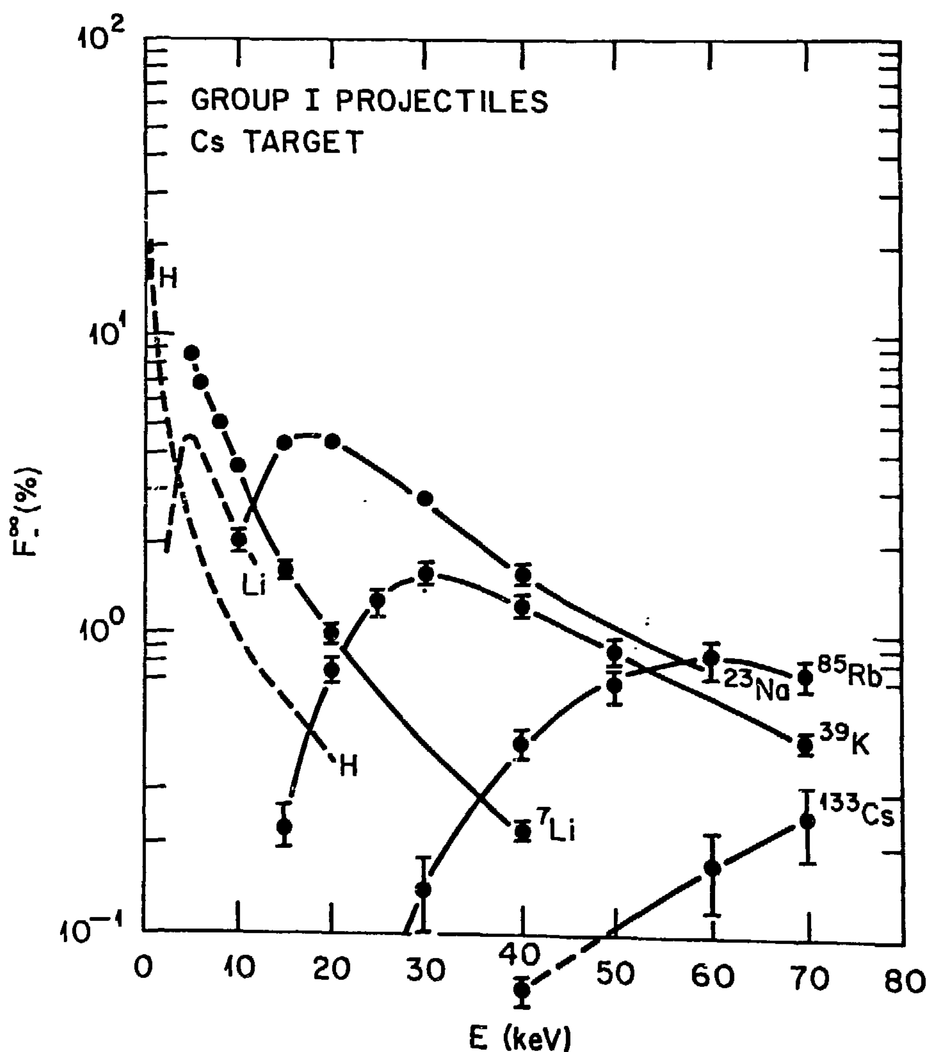

Fig. 9. Negative ion equilibrium yields F_-^∞ versus projectile energy E for various Group IA projectiles in Cs vapor (Ref. 58).

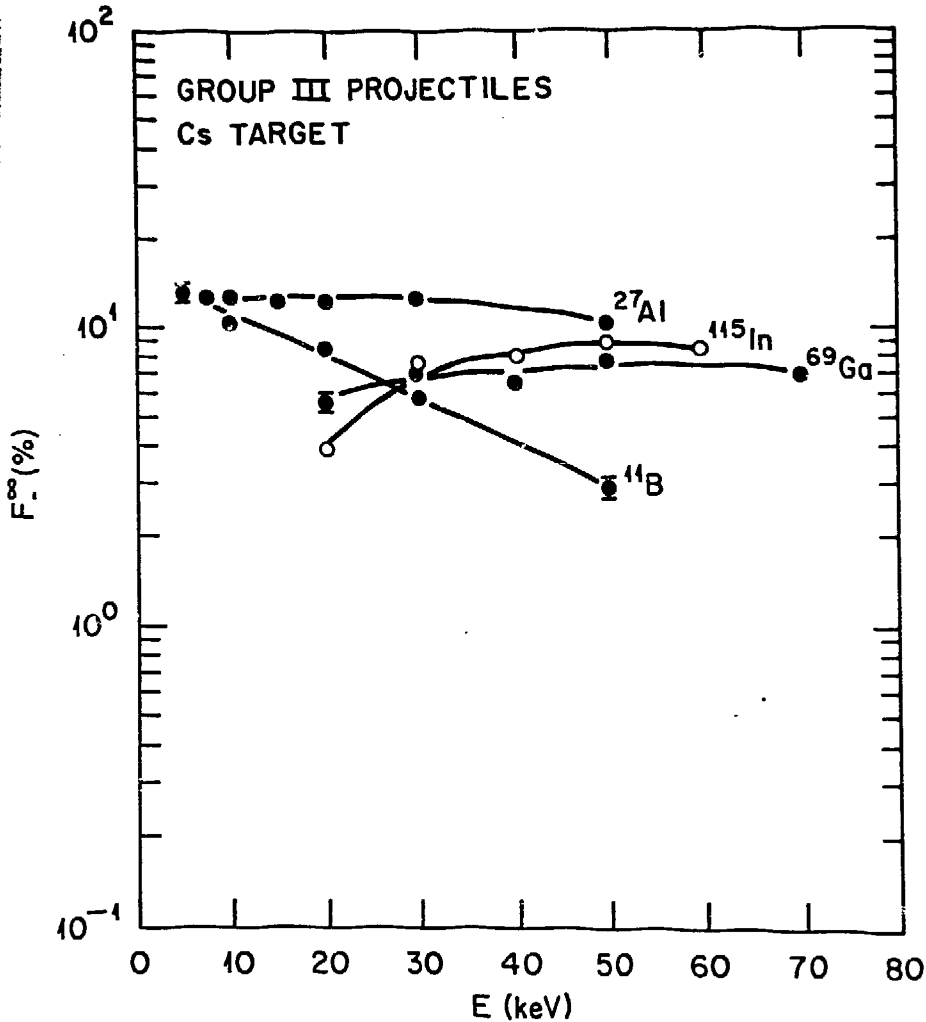

Fig. 10. Negative ion equilibrium yields F_-^∞ versus projectile energy E for various Group IIIA projectiles in Cs vapor (Ref. 58).

THERMODYNAMIC EQUILIBRIUM SURFACE IONIZATION

Atoms or molecules impinging on a hot metal surface may be emitted as positive or negative ions in subsequent evaporation processes after mean residence times τ_a and τ_i, respectively. The process of direct surface ionization is statistical in nature and therefore, statistical and thermodynamic arguments can be applied to such systems to derive equations for the degrees of positive or negative ion generation under thermodynamic equilibrium conditions. The subject has been reviewed in a comprehensive manner by Kaminsky[59] which contains many older review references on the subject.

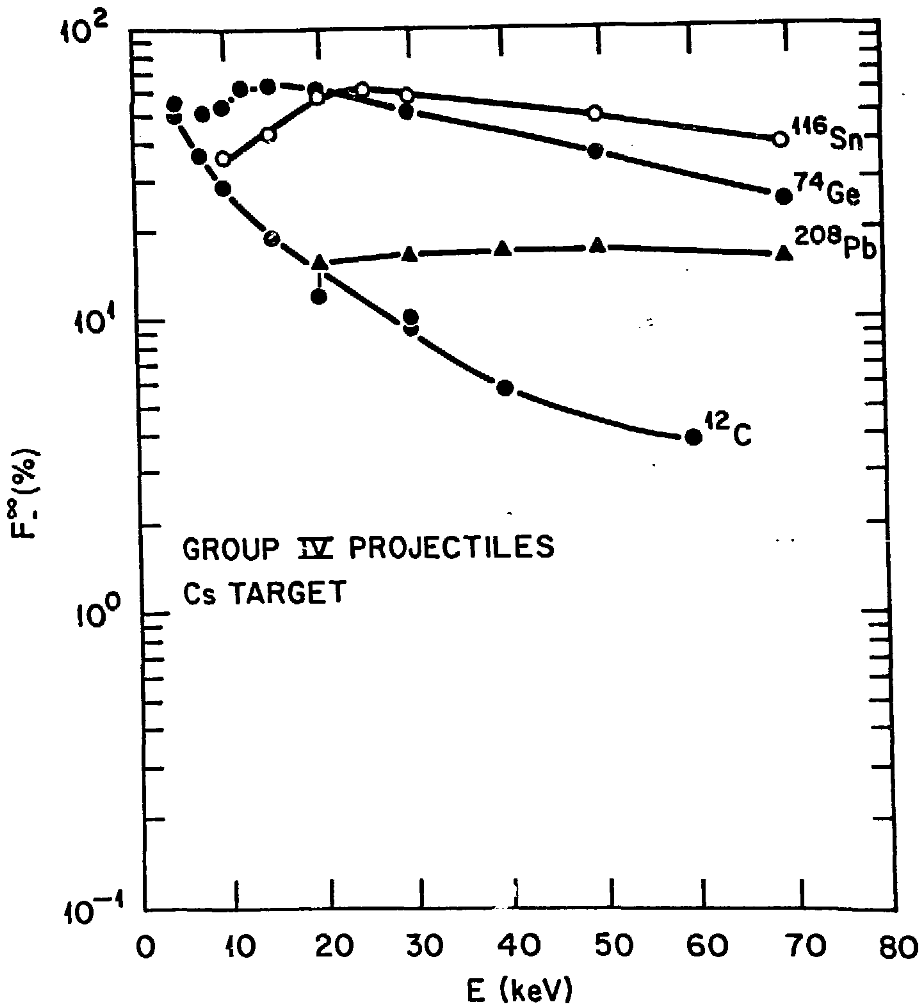

Fig. 11. Negative ion equilibrium yields F_-^∞ versus projectile energy E for various Group IVA projectiles in Cs vapor (Ref. 58).

The probability for arrival at a position far from the metal in a given state depends on the magnitude of the difference between the surface work function ϕ and the electron affinity E_A of the atom or molecule or $\phi - E_A$. For thermodynamic equilibrium processes, the ratio of ions to neutrals which leave an ideal surface can be predicted from Langmuir-Saha surface ionization theory. The form of the Langmuir-Saha equation for the probability of negative ion formation for neutral particles of electron affinity E_A interacting with a hot metal surface at temperature T and constant work function ϕ is given by

$$P_I = \frac{\frac{\omega_-}{\omega_o}\left(\frac{1-r_-}{1-r_o}\right)\exp(E_A-\phi)/kT}{1+\frac{\omega_-}{\omega_o}\left(\frac{1-r_-}{1-r_o}\right)\exp(E_A-\phi)/kT} \qquad (27)$$

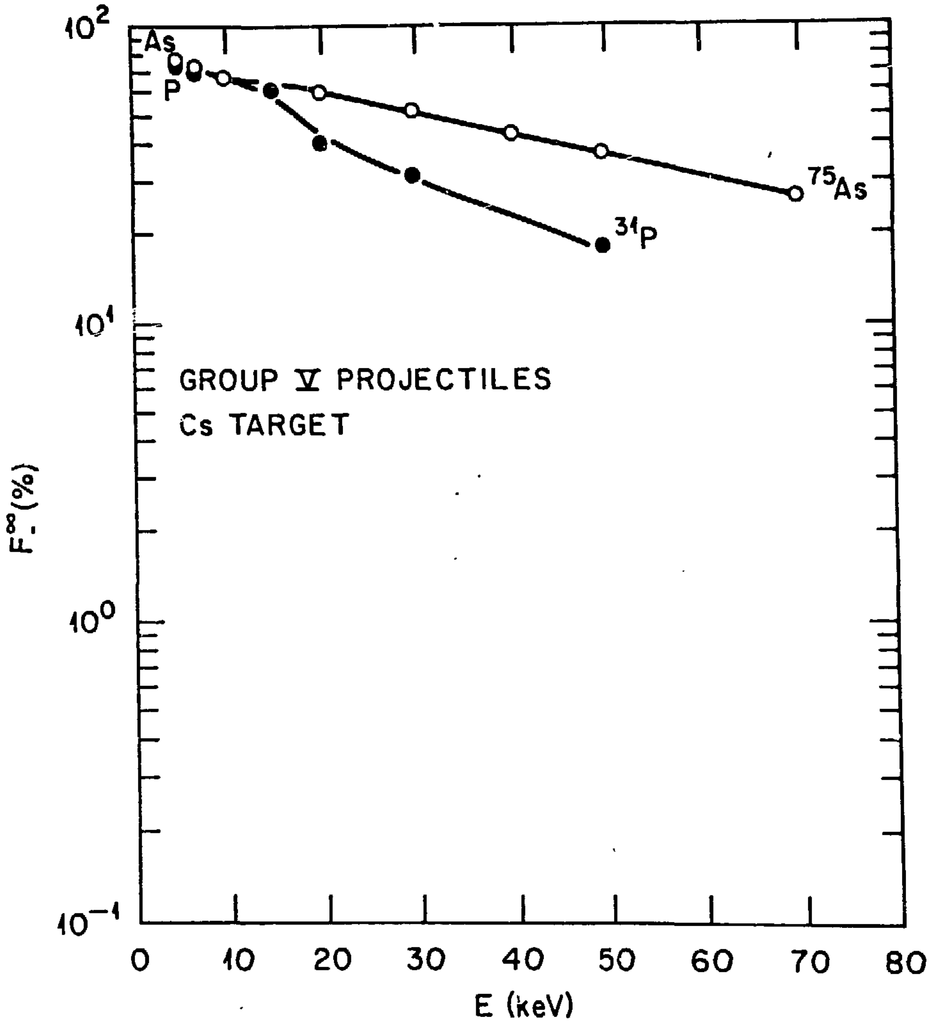

Fig. 12. Negative ion equilibrium yields F_-^∞ versus projectile energy E for As^+ and P^+ Group VA projectiles in Cs vapor (Ref. 58).

where r_-, r_0 are the reflection coefficients of the particle at the surface and ω_-, ω_0 are statistical weighting factors for the negative and neutral ion, respectively. ω_-, ω_0 are related to the total spin of the respective ion or neutral given by

$$\omega = 2\sum_i s_i + 1 \tag{28}$$

where s is the spin of the electron. Expression 27 is more complex in reality because of the variation of ϕ with crystalline orientation in cases where the metal is polycrystalline or the surface has uniformly or non-uniformly distributed surface contaminants. All of these effects can be taken into account by approximately summing over the admixtures of existing work functions and statistical weighting

factors in the respective expressions. From the relationships, it is evident that negative ion yields could be enhanced by lowering the work function ϕ, or by increasing the surface temperature T for elements where $E_A \leq \phi$. Negative surface ionization has not been utilized frequently as a means for practical production of ion beams – principally due to the lack of chemically stable low work function materials. A few examples, however, can be cited. These include the resistive heating of uranium metal[60] and carbon[61] to produce µA beams of UF_6^-. A source based on the use of LaB_6 has been described in Ref. 62. The source utilizes a porous graphite ionizer which is impregnated with LaB_6. A compound containing one of the halides is diffused through the low-work-function surface where it is ionized with high efficiency.

SECONDARY ION SURFACE IONIZATION

The processes for which the Langmuir-Saha relation apply are those which take place under thermodynamic or quasi-thermodynamic equilibrium. Such conditions are achievable for neutral particles incident on a surface at thermal energies where the sticking probabilities are approximately unity and consequently the residence time τ is long enough to approach thermodynamic equilibrium before evaporation occurs. However, the interactions involved in sputtering and ion scattering are not thermodynamic in nature and theories other than that of Langmuir-Saha are required for a proper description.

The probability that an atom will be ejected as an ion during a collision-induced cascade has been the subject of many investigations during the past several years. While considerable progress has been made toward a better understanding of negative ion formation by this process, the precise mechanism continues to be debated.[63-67] The key question is the role of the ejection velocity in the formation process. The probability for ion formation in models based upon local thermodynamic equilibrium (LTE) in the region of primary ion impact depends weakly on the ion ejection velocity.[67] On the other hand, theoretical treatments involving atomic excitation, leading to electron capture or loss, predict a strong velocity dependence for the secondary ion emission probability.[63-66] Theories have been developed which treat either negative ion formation in terms of an electron tunneling mechanism[64] or in terms of a velocity-dependent surface ionization mechanism.[65] Bond-breaking mechanisms have been proposed to explain secondary ion formation during sputtering of oxidized metal surfaces and atomic ion emission from molecular solids.[68-70] The simplest forms of the local thermodynamic equilibrium (LTE) approach to secondary ion emission are conceptually different from either the bond-breaking, the

electron tunneling, or the velocity-dependent surface ionization mechanism. The simple LTE models predict weak or no velocity dependence for the probability of ion emission,[67] while the bond-breaking mechanism,[68-70] electron tunneling,[64] and velocity-dependent surface ionization[65] mechanisms predict secondary ion emission that has an exponential velocity dependence.

Although several independent and distinct negative ion formation processes may coexist during sputtering, particularly from compound and alloyed samples, there is convincing evidence that the mechanism of formation during sputtering of "clean" metal surfaces is a form of surface ionization. In sources based on the sputter principle, positive ion beams, usually formed by either direct surface ionization of a group IA element or in a heavy noble gas (Ar, Kr or Xe) plasma discharge-seeded with alkali metal vapor, are accelerated to energies between a few hundred eV and several keV where they sputter a sample containing the element of interest covered with fractional layers of a highly electropositive adsorbate. Highly electropositive adsorbates such as the group IA elements dispersed on the surface of a metal greatly enhance the probability for negative ion formation by lowering the work function. This phenomenon makes possible the generation of a wide spectrum of negative ion beams in sources based on the sputter principle.[7]

Electropositive Adsorbate-Induced Work Function Changes It is well known that atomic adsorption of a dissimilar element on a clean surface affects the surface work function. The magnitude and sign of the change depends on the chemical properties of the adsorbed atom (adsorbate) and those of the host material (adsorbent). Electropositive atoms decrease the work function while electronegative atoms tend to increase the work function. The importance of surface adsorbates on negative ion formation processes has been realized since the discovery by Krohn that negative ion yields can be greatly enhanced by sputtering a material in the presence of an alkali metal.[71] The first direct correlation between negative ion yield and surface work function was made by Yu.[64]

Semiempirical relations have been proposed which relate the work function change $\Delta\phi$, in units of volts, V, to the surface coverage σ.[72–74] A simple analytical expression has been derived by Alton[74] which can be used to predict, with good accuracy, the value of the work function σ over the complete range of adsorbate coverage ($\sigma = 0$ to $\sigma = 1$). The equation which expresses the functional dependence of ϕ on σ can be written as follows:

$$\phi(\sigma) = \phi_o + \frac{6\Delta\phi_m}{(3-\sigma_m)\sigma_m}\sigma - \frac{3\Delta\phi_m(\sigma_m+1)}{(3-\sigma_m)\sigma_m^2}\sigma^2 + \frac{2\Delta\phi_m}{(3-\sigma_m)\sigma_m^2}\sigma^3 [V], \tag{29}$$

where ϕ_o is the intrinsic work function of the surface at $\sigma = 0$ and $\Delta\phi_m$ is the maximum change in work function which occurs at a relative adsorbate coverage value of $\sigma = \sigma_m$. The expression which gives the maximum change $\Delta\phi_m$ in the work function at σ_m is given by

$$\Delta\phi_m \equiv -1.24\left[\phi_o - \frac{1}{2}(i_A + E_A)\right][V], \tag{30}$$

where I_A is the first ionization potential and E_A the electron affinity of the adsorbate material. Expression 30 reproduces, with good accuracy, maximum work function changes observed for alkali and alkaline earth metal adsorbates.[74]

<u>Theoretical Negative Ion Current</u> If we ignore collisional detachment processes and interference to sputtering of sample atoms by surface adsorbate atoms, the negative ion current I^- can be expressed by the following simple relationship:

$$I^- = 2\pi I^+(E_1)S(E_1,\theta_i)\int_{V_i}^{E'}\int_0^{\pi/2} P^-(E_2,\theta)f(E_2,\theta)\sin\theta d\theta dE_2, \tag{31}$$

where I^+ is the incident positive ion current of energy E_1, $S(E_1, \theta_i)$ is the sputter ratio of the target at projectile energy E_1 and angle of incidence with respect to the surface normal θ_i, $f(E_2, \theta)$ is the neutral atom energy-angular distribution function and $P^-(E_2, \theta)$ is the probability for negative ion formation for atoms ejected at energy E_2 and polar angle θ with respect to the surface normal. The limits of integration over energy E_2 are taken between V_i, the image potential induced in the surface by the departing negative ion, and E', the maximum energy transfer that can occur between a projectile of energy E_1 and mass M_1 and a target atom of mass M_2. E' is given by the relation

$$E' = \frac{4M_1M_2}{(M_1+M_2)^2}E_1. \tag{32}$$

<u>The Nørskov and Lundqvist Model</u> Nørskov and Lundqvist[65] determined expressions for positive- and negative-ion emission probabilities $P^+(\upsilon_\perp)$ and $P^-(\upsilon_\perp)$ as a function of the perpendicular component of the ejection velocity of the particle with respect to the surface, $\upsilon_\perp$. For purposes of the present paper, we are only interested in $P^-(\upsilon_\perp)$.

In the prescription of Ref. 65, the probability for negative ion formation can be cast into a simple energy-dependent form given by

$$P^{-}(E_2,\theta)=\frac{2}{\pi}\exp\left\{\frac{-\beta\sqrt{M_2}\left[\phi(\sigma)-E_A+V_i\right]}{\sqrt{2E_2}\cos\theta}\right\}, \tag{33}$$

where ϕ is the work function of the surface (ϕ depends on the relative adsorbate coverage σ), E_A is the electron affinity of the ejected particle of mass M_2 and energy E_2, V_i is the image potential induced in the surface by the escaping ion, θ is the polar angle of the sputtered ion with respect to the surface normal and β is a constant. In Eq. 33, $\sqrt{2E_2/M_2}\cos\theta = v_{\perp}$, is the component of the velocity of the escaping particle perpendicular to the metal surface. The mechanism for ion formation based on this theory is a velocity-dependent form of surface ionization. Experimental evidence in support of the velocity dependence of the secondary ion formation process has been provided by Yu for negative ions[75] and by Vasile for positive ions.[76]

The Energy-Angular Distribution Function Under the assumption of isotropic collision cascades and a planar surface potential E_b, linear cascade theory predicts the following energy-angular distribution function for sputter-ejected atoms:[77]

$$f_m(E_2,\theta)=A_m\frac{E_2\cos\theta}{(E_2+E_b)^{3+2m}}, \tag{34}$$

where E_2 is the energy of the ejected particle, θ is the polar angle with respect to the normal of the surface and m is the power potential parameter. The maximum in the distribution occurs at $E_{max} = E_b/(2-2m)$ and is independent of the emission angle θ. For the low energies appropriate for sputtering, m is found to be close to zero.[78,79] The resulting expression,

$$f_0(E_2,\theta)=\frac{A_0E_2\cos\theta}{(E_2+E_b)^3}, \tag{35}$$

was first developed by Thompson[77] and is often referred to as the Thompson model.

Computed Negative Ion Energy Distribution Functions The Nørskov and Lundqvist model is assumed valid for purposes of illustration. Figure 13 shows the energy distribution of neutral and negative ions sputtered from a Mo surface at four surface coverages σ as determined by integrating, respectively, the Thompson relation and the product of the Thompson and the Nørskov and Lundqvist relation over the complete range of polar angle $0 \leq \theta \leq \pi/2$. We use Eq. 29 to simulate the work function ϕ versus relative cesium coverage σ. The parameter β was obtained from the fits to the Yu data

of Ref. 64 with $V_i = 1.4$ eV, the electron affinity E_A and intrinsic work function ϕ_o for Mo were used in Eq. 29 for calculating the work function ϕ at a particular cesium surface coverage σ. We note that the peaks in the negative ion energy distribution functions shift toward lower energies as the work function ϕ is lowered and reach the left-most position when $\sigma = 0.5$; at higher relative coverages, the distributions shift toward the right-hand side of the energy scale. The maximum probability for negative ion formation occurs for a cesium adsorbate coverage of $\sigma = 0.5$, in keeping with the observations of Yu.[64] Thus, the energy distributions of secondary negative ions in the energy-dependent prescription of Nørskov and Lundqvist are seen to be sensitive in shape and position to the surface work function ϕ at adsorbate coverage σ. The effect of work function changes on secondary ion energy spectra have also been discussed by Wittmaack.[80] The extreme velocity dependence predicted by this theory is now being seriously challenged.

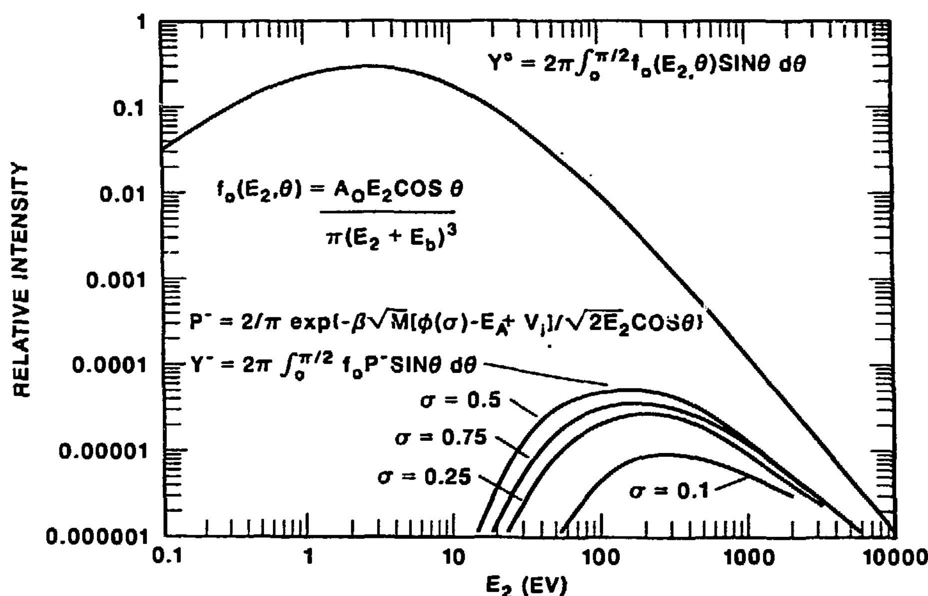

Fig. 13. Energy distributions of sputtered Mo neutral atoms and Mo⁻ ions calculated by integrating the Thompson relation[77] (Eq. 35) and the product of the Thompson[77] and Nørskov and Lundqvist[65] relations over all azimuthal and polar angles, respectively. The parameter β was determined by fitting to the Mo⁻ versus relative cesium coverage data of Yu[64] with an assigned value for $V_i = 1.4$ eV. Four relative cesium coverage values were used: $\sigma = 0.1$, $\sigma = 0.25$, $\sigma = 0.50$, and $\sigma = 0.75$.

Computed Total Probabilities for Negative Ion Formation In order to determine the total probability for negative ion formation at a particular surface coverage, one must integrate Eq. 33 over the complete range of particle ejection energies E_2 and over all

polar angles θ. Figure 14 displays the total probability P_T^- versus the cesium surface coverage σ for the case when the Thompson relation is used.

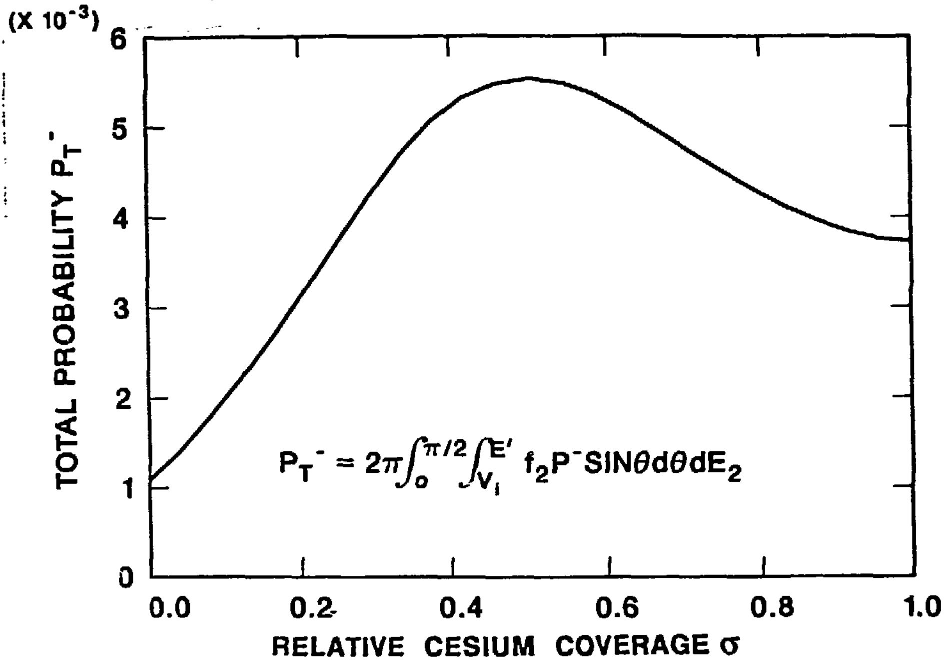

Fig. 14. Calculated total probability P_T^- for Mo^- formation versus relative cesium coverage σ. The total probability P_T^- was determined by integrating the product of the Nørskov and Lundqvist relation[65] (Eq. 33) and the Thompson relation[77] (Eq. 35) over the complete energy range $V_i \leq E_2 \leq E'$ with image potential $V_i = 1.4$ eV and E′ given by $E' = 4M_1M_2E_1/(M_1 + M_2)^2$. The parameter β of Eq. 33 was determined by fitting to the experimental data of Yu.[64] The Alton model[74] (Eq. 29) was used to estimate the work function of the Mo surface at a particular cesium coverage σ.

The Local Thermodynamic Equilibrium (Sroubek) Model

The Nørskov and Lundqvist non-thermodynamic velocity-dependent surface ionization model was developed for the situation appropriate for a broad valence band atom ejected from a solid in which the Fermi distribution is not disturbed. In this model, the atomic level of the sputtered particle varies rapidly with distance z from the surface. According to this model, the probability for ionization $P^{\pm}$ depends exponentially on the width of the atomic level Δ (z_c) and on the perpendicular component of velocity $v_\perp$ at the point at which the atomic level crosses the Fermi level z_c according to

$$P^{\pm} = \exp\left[-2\Delta(z_c)/\hbar\gamma v_\perp(z_c)\right] \quad (36)$$

where γ is the characteristic decay length. This relation assumes that the atomic level Δ decreases exponentially with distance z from the surface. Therefore, the probability

P± depends on the assumptions made for the functional dependence of Δ and the way that ε_A varies with distance as well.[66,81] The velocity dependence of Eq. 36 has been verified for high probability processes.[75,76] However, if the level width Δ is assumed to vary linearly, a power law dependence results.[66,82] The power law dependence is consistent with excitation of electrons within the solid and, therefore, is more important in low probability processes. The model described by Eq. 36 does not include excitations of the Fermi distribution of electrons within the solid which, if excited, enhance the probability of capture to the sputter ejected atom. The Sroubek LTE model[82] neglects non-adiabatic transfer of continuum electrons to and from the sputter-ejected atom, but includes excitation of the electrons within the solid with effective energy kT_S. Under these assumptions, Sroubek LTE derives the following expression for the negative ionization process:

$$P^- = \exp\left[-\frac{E_A - \phi}{kT_s}\right]. \tag{37}$$

<u>The Modified Surface Ionization Model</u> Although basic surface ionization theory is, in the strictest sense, only applicable to systems in thermodynamic equilibrium and the sputtering process does not meet this criterion, a modified form of the Langmuir-Saha relation was found to reproduce maximum negative ion yields from a plasma-type negative ion source.[83] In an early study, this model was found to reproduce negative ion yields on a relative basis for a wide range of elements. In this treatment, kT_s was found to be a constant and independent of species.

In this model, the probability of a particle leaving a surface as a negative ion is given by

$$P^- = \frac{\frac{\omega_-}{\omega_0}\left[\frac{1-r_-}{1-r_0}\right]\exp(E_A - \phi)/kT_s}{1+\frac{\omega_-}{\omega_0}\left[\frac{1-r_-}{1-r_0}\right]\exp(E_A - \phi)/kT_s} \tag{38}$$

where r_-, r_0 are surface reflection coefficients of the negative and neutral particles, respectively, E_A is the atomic electron affinity of the target material, k is Boltzmann's constant, T_S is the effective temperature of the surface, ω_- and ω_0 are statistical weighting factors which are related to the total electronic spin of the respective species given by Eq. 28 and ϕ is the value of the work function at optimum surface coverage previously defined by Eq. 30. The reflection coefficients r_- and r_0 are assumed to be identical. This model is then identical to the Sroubek LTE model[82] with the exception

of the multiplication ω_-/ω_0 factor, which is usually 1 or 2, depending on the net spin of the negative and neutral components.

Comparisons of the relative probabilities estimated from negative ion source yield data taken from the source described in Ref. 83 and values computed for P^- from the modified surface ionization model in conjunction with work function changes $\Delta\phi_m$ computed from Eq. 30 are shown in Table III. The probability of ion extraction from the source is assumed to be unity. The probabilities P^- (meas.) were determined from measured values of momentum-analyzed negative ion currents, nominal cathode sputter ion currents, cathode voltages, and calculated normal incident ion sputter ratios. The effective temperature T_s of the surface is found to be independent of source operating conditions and assumed to be associated with the sputter process itself. A steady state value of 673K was found to best fit the data for the modified surface ionization model. This value is obviously much too low in relation to typical energies of negative ions generated by sputtering. Neither the Sroubek model[82] nor the modified surface ionization model[83] incorporates the image potential V_i which must be overcome by the escaping ion. Incorporation of an image potential (typically $V_i = 1.4$ eV) which is additive to the work function value would increase the effective temperature of the surface.

Experimental Results Related to Non-thermodynamic Equilibrium Negative Ion Generation - Temperature Effects One of the key questions related to negative ion generation by sputtering is whether or not sputter-generated negative ion yields are dependent on the sample temperature in the sense predicted by the Langmuir-Saha relation (Eq. 27). Measurements of negative ion yields versus sample temperature during sputtering of samples mounted in negative ion sources have been made by Alton[84] and Takeiri.[85] Figures 15 and 16 display total negative ion yields versus sample temperature for carbon and copper samples as measured in a refocus geometry cesium sputter negative ion source.[84]

As noted, the carbon data appear to have a very weak temperature dependence, while those for copper appear to be essentially independent of temperature over the ranges indicated. From these data, we conclude that negative ion yields are only marginally affected by sample temperature. The moderate temperature dependence for the total negative ion yields from the carbon sample are believed to be associated with the redistribution of C_2^-, C_3^-, and higher-order components with sample temperature. It, thus, appears that negative ion formation by sputter ejection is not

strongly dependent on the sample temperature, at least below 400°C for carbon and 200°C for copper. At much higher temperatures, however, there is loss of cesium at the surface through thermal evaporation.[85]

TABLE III Calculated and observed relative negative ionization probabilities: Modified surface ionization model.

Ion Species	ϕ_0(eV)	E_A(eV)	$P^-_{(meas)}$	$P^-_{(calc)}$
C^-	4.39	1.268	2.67×10^{-3}	2.5×10^{-3}
V^-	4.11	0.5	4×10^{-5}	3.8×10^{-10}
Co^-	4.18	0.7	1.35×10^{-4}	1.5×10^{-8}
Ni^-	4.84	1.15	1.77×10^{-3}	2.13×10^{-3}
Cu^-	4.47	1.226	1.32×10^{-3}	1.3×10^{-3}
Nb^-	3.99	1.0	6.67×10^{-5}	1.21×10^{-6}
Mo^-	4.27	1.0	2×10^{-5}	1.6×10^{-5}
Ag^-	4.28	1.303	5.7×10^{-4}	7.4×10^{-4}
Sn^-	4.11	1.25	5.3×10^{-4}	5.8×10^{-4}
Sb^-	4.08	1.05	4.5×10^{-5}	4.14×10^{-6}
Ta^-	4.12	0.6	4×10^{-6}	2×10^{-9}
W^-	4.52	0.6	4.7×10^{-5}	4×10^{-8}
Pb^-	4.02	1.1	2×10^{-5}	3×10^{-5}

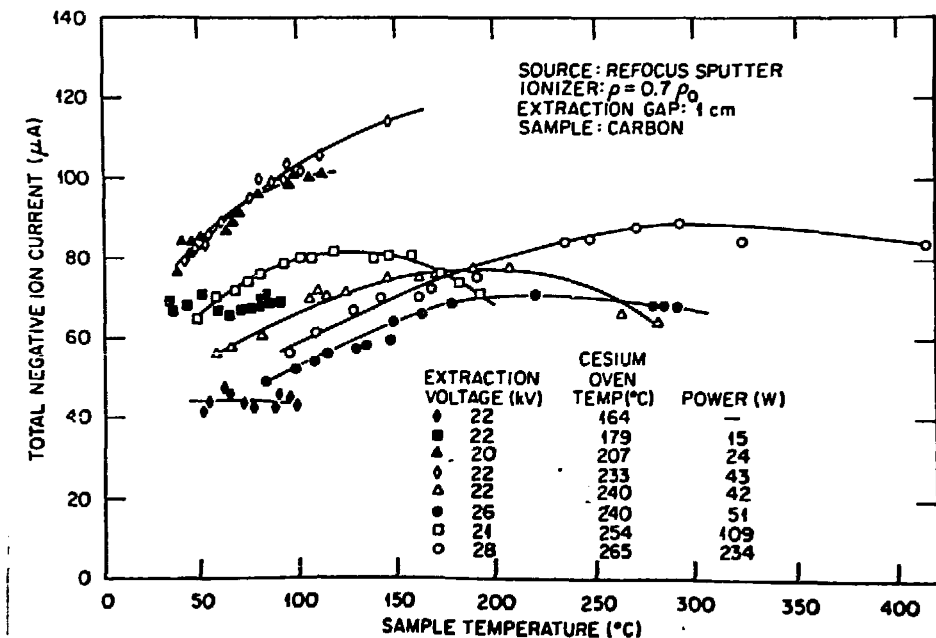

Fig. 15. Total negative ion yields from a carbon sample vs sample surface temperature with cesium ion beam power as a parameter (Ref. 84).

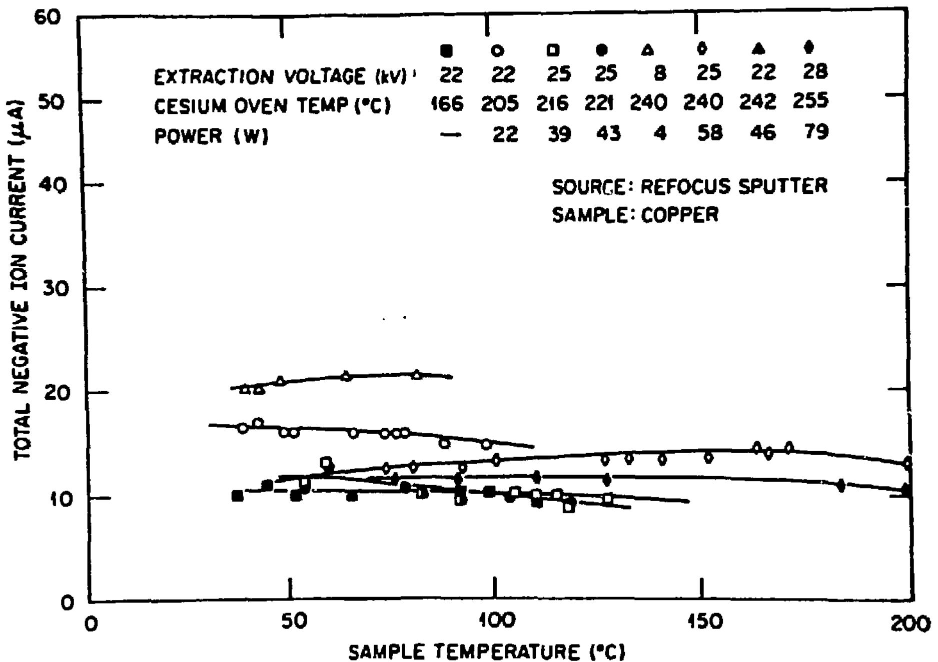

Fig. 16. Total negative ion yields from a copper sample vs sample surface temperature with cesium ion beam power as a parameter (Ref. 84).

However, materials which have low thermal conductance, such as boron, can reach sufficiently high temperatures during bombardment to affect negative ion yields. These findings are also consistent with the constant temperature value required by the modified surface ionization model to fit maximum negative ion yields, regardless of species, extracted from a sputter-type plasma sputter negative ion source.[83]

Experimental Probabilities for Negative Ion Formation During Sputtering The absolute probability for negative ion formation during sputtering is difficult to quantify on an absolute basis. Effective probabilities versus extraction voltage for generation of total negative ion beams in a refocus-geometry cesium negative ion source have been measured by Alton.[84] The results obtained for carbon and copper samples are displayed in Figs. 17 and 18.

Negative ion yields versus cesium ion beam intensity have been measured by Takeiri[85] using a high-intensity source developed by Ishikawa and colleagues.[86] The results of $^{12}C^-$ and $^{11}B^-$ ion currents versus Cs^+ target ion current as measured by Takeiri are displayed in Figs. 19 and 20, respectively. The data for both processes exhibit constant efficiencies over a wide range of values. These data also reflect the effect of cooling the sample. If the sample surface is too cool as reflected by the C^- data when liquid nitrogen or liquid CO_2 is used, the efficiency of ion formation is

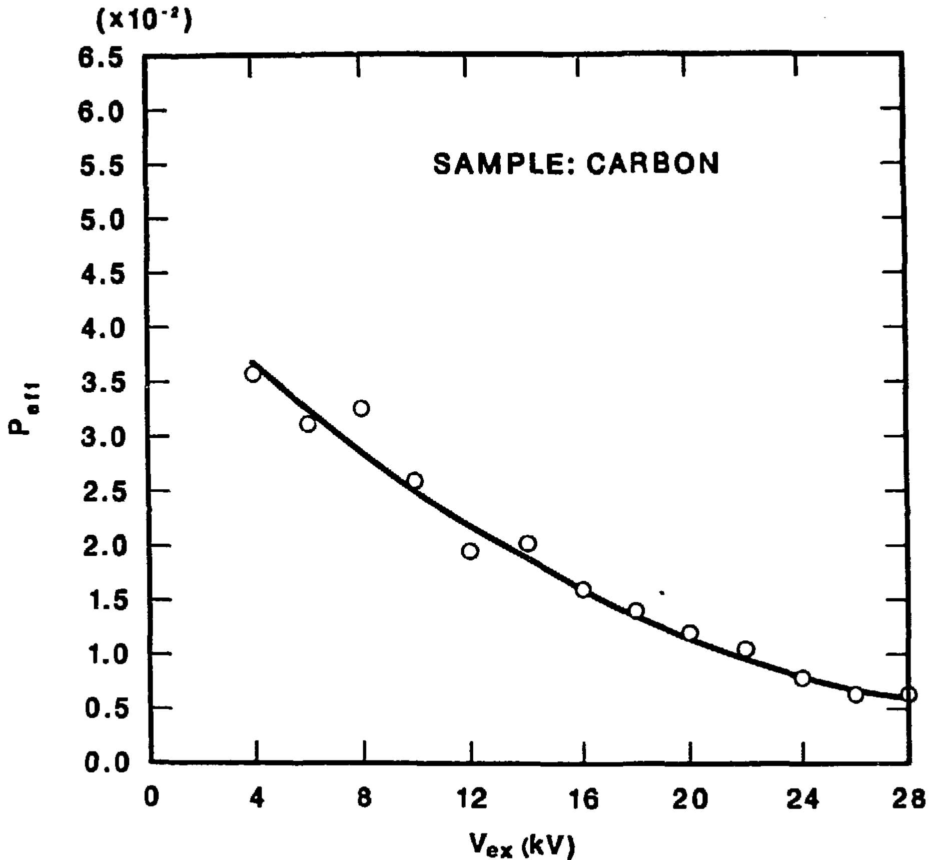

Fig. 17. Effective probability P_{eff} for generating and extracting negative ions from a carbon sample in the refocus geometry negative ion source as a function of extraction voltage, V_{ex}, at optimum cesium oven temperature (Ref. 84).

reduced. This is more than likely a result of condensation of too much cesium on the surface, which interferes with the ejection of carbon atoms during the sputter process. On the other hand, when liquid nitrogen or liquid CO_2 target coolant is used, the efficiency for $^{11}B^-$ ion formation from sintered boron samples is enhanced. This effect is attributable to the fact that boron has a low thermal conductivity and that the sample temperature reaches values high enough to thermally evaporate cesium at a rate sufficient so that optimum cesium surface coverage cannot be maintained.

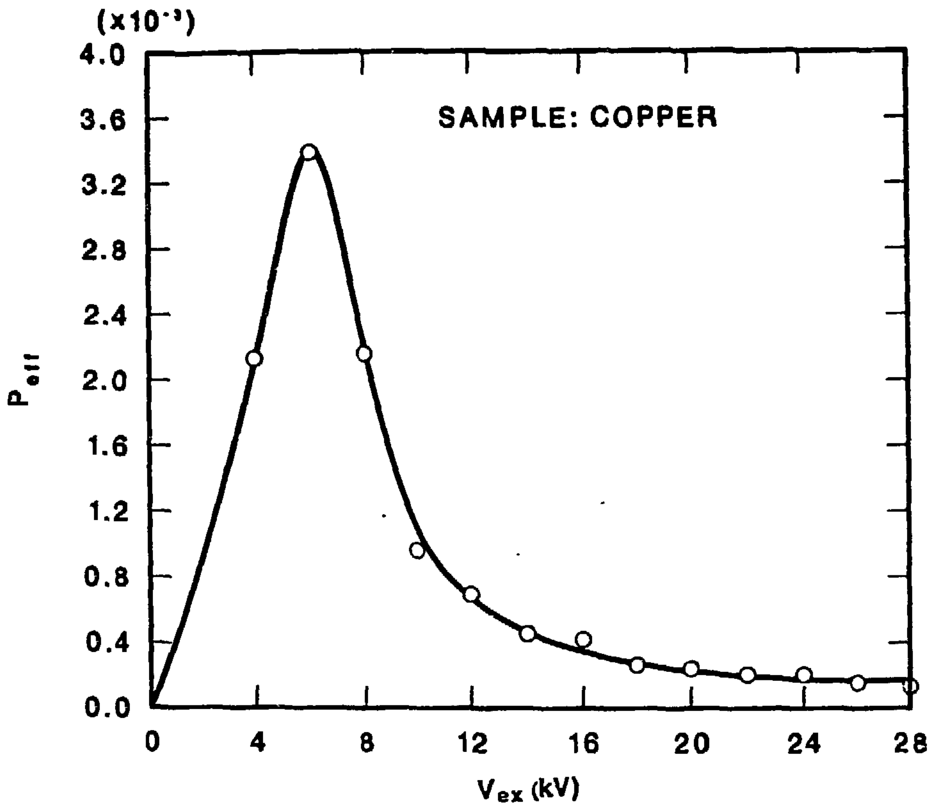

Fig. 18. Effective probability P_{eff} for generating and extracting negative ions from a copper sample in the refocus geometry negative ion source as a function of extraction voltage, V_{ex}, at optimum cesium oven temperature (Ref. 84).

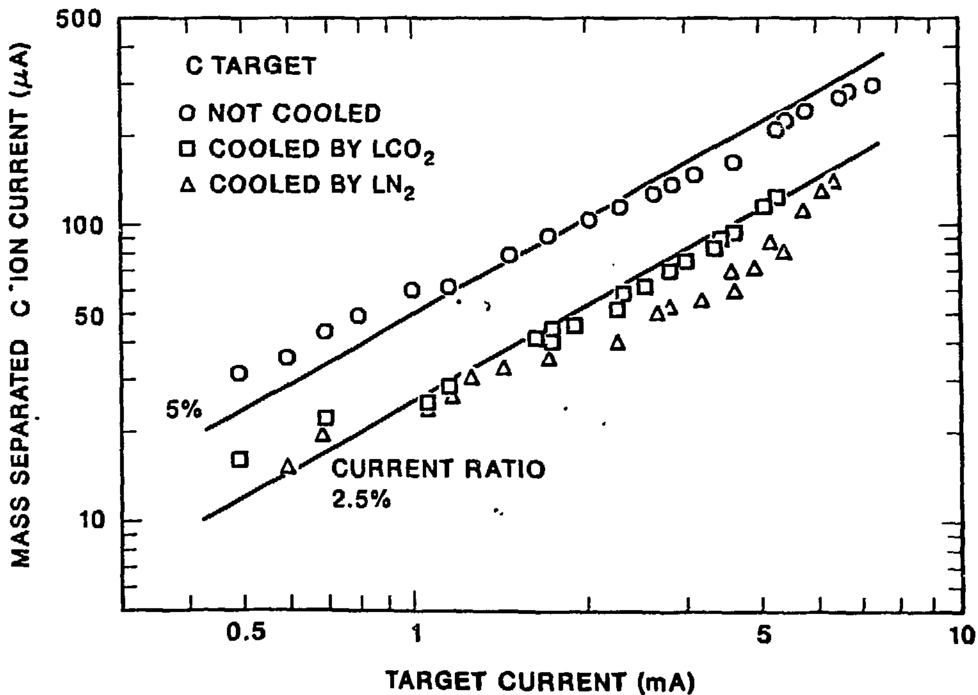

Fig. 19. Mass separated $^{12}C^{-}$ ion current versus sputter target current showing the effect of target cooling on negative ion production efficiency (Ref. 85).

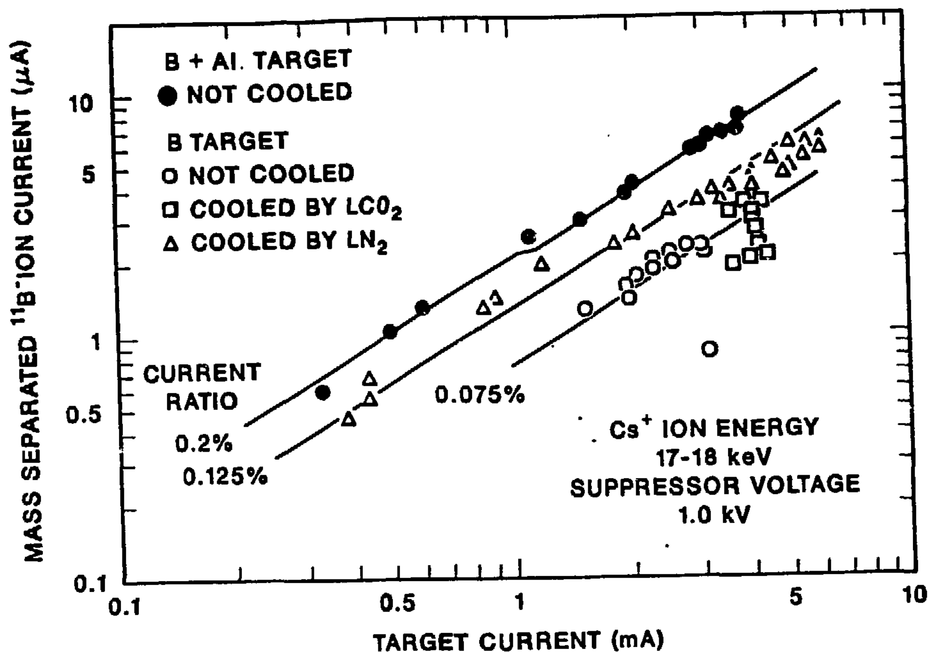

Fig. 20. Mass separated $^{11}B^-$ ion current versus sputter target current showing the effect of target cooling on negative ion production efficiency (Ref. 85).

ACKNOWLEDGEMENTS

The author is indebted to Ms. Jeanette McBride for typing and preparation and to Dr. C. M. Jones for editing the manuscript.

REFERENCES

1. T. B. Clegg, Proc. Conf. on Polarized Proton Ion Sources, AIP Conf. Proc. 117 (1984) 63.
2. Y. Mori, A. Takagi, K. Ikegami, S. Fukumoto, A. Ueno, C. D. P. Levy, and P. W. Schmor, AIP Conf. Proc. 158 (1987) 605.
3. L. W. Anderson, Nucl. Instrum. and Meth. 167 (1979) 363.
4. A. N. Zelenskii, S. A. Kokhanovskii, V. M. Lobashev, and V. G. Polushkin, JETP Lett. 42 (1985) 5.
5. W. Grüebler, Proc. Conf. on Polarized Proton Ion Sources, AIP Conf. Proc. 117 (1984) 1.
6. G. D. Alton, Ionization Phenomena and Sources of Ions, Chap. 2, Vol. 4 in Applied Atomic Collisions Physics, Edited by H. W. Massey (Academic Press, Inc., New York).
7. G.D. Alton, IEEE Cat. No. 89CH2669-0, Vol. 2 (1989) 1112.
8. H. S. W. Massey, Negative Ions, (Cambridge University Press, London, 1976).
9. B. M. Smirnov, Negative Ions, (McGraw-Hill, New York, 1982).
10. H. Hotop and W. C. Lineberger, J. Phys. Chem. Ref. Data 4 (1975) 539.
11. T. J. Kvale, G. D. Alton, R. N. Compton, D. J. Pegg, and J. S. Thompson, Phys. Rev. Lett. 55 (1985) 484.
12. D. J. Pegg, J. S. Thompson, R. N. Compton, and G. D. Alton, Phys. Rev. Lett. 59 (1987) 2267.
13. C. F. Fischer, Phys. Rev. A39 (1989) 963.
14. K. M. Griffing and J. Simons, J. Chem. Phys. 64 (1976) 3610.

15. D. E. Jensen, Trans. Faraday Soc. 65 (1969) 2123.
16. K. D. Jordan, K. M. Griffing, J. Kenney, E. L. Andersen, and J. Simons, J. Chem. Phys. 64 (1976) 4730.
17. J. Berkowitz, W. A. Chupka, and T. A. Walter, J. Chem. Phys. 50 (1969) 1497.
18. P. C. Engelking and W. C. Lineberger, J. Chem. Phys. 66 (1977) 5054.
19. D. K. Jordan and J. Simons, J. Chem. Phys. 65 (1976) 1214.
20. P. C. Engelking and W. C. Lineberger, J. Chem. Phys. 65 (1976) 4323.
21. D. Feldman, Z. Naturforsch A25 (1970) 621.
22. D. G. Hopper, A. C. Wahl, R. L. C. Wu, and T. O. Tiernan, J. Chem. Phys. 65 (1976) 5474.
23. P. Warneck, Chem. Phys. Lett. 3 (1969) 532.
24. J. Beauchamp, J. Chem. Phys. 64 (1976) 929.
25. B. P. Mathur, E. W. Rothe, and G. P. Reck, J. Chem. Phys. 67 (1977) 377.
26. A. V. Bunge and C. F. Bunge, Phys. Rev. A19 (1979) 452.
27. G. D. Alton, R. N. Compton, and D. J. Pegg, Phys. Rev. A28 (1983) 1405.
28. L. M. Blau, R. Novick, and D. Weinflash, Phys. Rev. Lett. 24 (1970) 1268.
29. R. Novick and D. Weinflash, Proc. Int. Conf. Precision Measurements and Fundamental Constants (Gaithersburg, MD 1970), eds. D. N. Langenberg and B. N. Taylor, Natural Bureau of Standards Spec. Publication No. 343 (1971) 403.
30. T. J. Kvale, R. N. Compton, G. D. Alton, J. S. Thompson, and D. J. Pegg, Phys. Rev. Lett. 56 (1986) 592.
31. J. Franck, Trans. Faraday Soc. 21 (1925) 536.
32. E. V. Condon, Phys. Rev. 32 (1928) 858.
33. K. N. Leung, Nucl. Instrum. and Meth. B 40/41 (1989) 1028.
34. D. Rapp and W. E. Francis, J. Chem. Phys 37 (1962) 2631.
35. W. L. Fite, R. F. Stebbings, D. G. Hummer, and R. T. Brackmann, Phys. Rev. 119 (1960) 663.
36. A. Dalgarno and H. N. Yadav, Proc. Phys. Soc., Lond. A66 (1953) 173.
37. J. B. Hasted and J. B. H. Stedeford, Proc. Roy. Soc. A277 (1955) 466.
38. P. Pradel, F. Roussel, A. S. Schlachter, G. Spiess, and A. Valence, Phys. Rev. A 10 (1974) 797.
39. F. Roussel, P. Pradel, and G. Spies, Phys. Rev. A 16 (1977) 1854.
40. V. N. Tuan, G. Gautherin, and A. S. Schlachter, Phys. Rev. A 9 (1974) 1242.
41. F.Brouillard, W. Claeys, and G. Van Wassenhove, J. Phys. B 10 (1977) 687; and X ICPEAC (Paris, 1977) 1264.
42. T. Nagata, J. Jpn. Soc. 46 (1979) 1622.
43. T. J. Morgan and F. Eriksen, Phys. Rev. A19 (1979) 2185.
44. M. Mayo, J. Stone, and T. J. Morgan, 1983
45. H. S. W. Massey, Rep. Progr. Phys. 12 (1949) 248.
46. J. B. Hasted, Proc. Roy. Soc. A205 (1951) 421; A212 (1952) 235.
47. G. D. Alton,T. J. Kvale, R. N. Compton, D. J. Pegg, and J. S. Thompson, Nucl. Instrum. and Meth. A 244 (1986) 142.
48. R. H. McFarland, A. S. Schlachter, J. W. Stearns, B. Liu, and R. E. Olson, Phys. Rev. A26 (1982) 775.
49. A. S. Schlachter, AIP Conf. Proc. No. 117 (1984) 180.
50. G. I. Dimov and G. V. Roslyakov, Instr. Expl. Tech. 17 (1974) 658.
51. R. J. Girnius, C. J. Anderson, and L. W. Anderson, Phys. Rev. A16 (1977) 2225.
52. B. A. D'Yachkov and V. I. Zinenko, Sov. Phys. – Tech. Phys. 16 (1971) 305.
53. R. M. Ennis, Jr., D. E. Schechter, G. Thoeming, D. B. Schlafke, and B. L. Donnally, IEEE Trans. Nucl. Sci. NS-14 (1967) 75.
54. R. J. Girnus and L. W. Anderson, Nucl. Instrum. and Meth. 137 (1976) 373.
55. A. S. Schlachter, D. H. Loyd, P. J. Bjorkholm. L. W. Anderson, and W. Haeberli, Phys. Rev. 174 (1968) 201.

56. J. Heinemeier and P. Hvelplund, Nucl. Instrum. and Meth. 148 (1975) 65.
57. J. Heinemeier and P. Hvelplund, Nucl. Instrum. and Meth. 148 (1975) 425.

58. T. J. L. Greenway (deceased) private communication.
59. M. Kaminsky, Atomic and Ionic Impact Phenomena on Metal Surfaces (Springer Verlag, New York, 1965).
60. R. N. Compton, P. W. Reinhardt, and W. R. Garrett, J. Chem. Phys 66 (1977) 4712.
61. P. F. Dittner and S. Datz, J. Chem. Phys. 68 (1978) 2451,
62. N. Kashihira, E. Vietzke, and G. Zellermann, Rev. Sci. Instrum. 48 (1977) 171.
63. A. Blandin, A. Nourtier, and D. W. Hone, J. Phys. (Paris) 37 (1976) 369.
64. M. L. Yu, Phys. Lett. 40 (1978) 574.
65. J. K. Nørskov and B. I. Lundqvist, Phys. Rev. B19 (1979) 5661.
66. G. Blaise and A. Nourtier, Surf. Sci. 90 (1979) 495.
67. Z. Sroubek, Phys. Rev. B25 (1982) 6046.
68. M. L. Yu, Nucl. Instrum. and Meth. B18 (1987) 542.
69. P. Williams, Surf. Sci. 90 (1979) 588.
70. G. Slodzian, Surf. Sci. 48 (1975) 161.
71. V. E. Krohn, Jr., Appl. Phys. 33 (1962) 3523.
72. J. Topping, Proc. Roy. Soc., London A114 (1927) 67.
73. E. P. Gyftopoulos and J. D. Levine, J. Appl. Phys. 33 (1962) 67.
74. G. D. Alton, Surf. Sci. 175 (1986) 226.
75. M. L. Yu, Phys. Rev. Lett. 47 (1981) 1325.
76. M. J. Vasile, Phys. Rev. B29 (1984) 3785.
77. M. W. Thompson, Philos. Mag. 18 (1968) 377.
78. J. P. Biersack and W. Eckstein, Appl. Phys. 34 (1984) 73.
79. M. T. Robinson, J. Appl. Phys. 54 (1983) 2650.
80. K. Wittmaack, Phys. Scripta T6 (1983) 71.
81. A. Nourtier, J. P. Jardin, and J. Quazza, Phys. Rev. B37 (1988) 10628.
82. Z. Sroubek, Nucl. Instrum. and Meth. 194 (1982) 533.
83. G. D. Alton and G. C. Blazey, Nucl. Instrum. and Meth. 166 (1979) 105.
84. G. D. Alton, Rev. Sci. Instrum. 59 (1988) 1045.
85. Y. Takeiri, Intense Heavy Negative Ion Beam Production and Negative Ion Beam Deposition, Ph.D. dissertation, Kyoto University, 1987.
86. J. Ishikawa, Y. Takeiri, and T. Takagi, Rev. Sci. Instr. 57 (1986) 1512.

DISCLAIMER

This report was prepared as an account of work sponsored by an agency of the United States Government. Neither the United States Government nor any agency thereof, nor any of their employees, makes any warranty, express or implied, or assumes any legal liability or responsibility for the accuracy, completeness, or usefulness of any information, apparatus, product, or process disclosed, or represents that its use would not infringe privately owned rights. Reference herein to any specific commercial product, process, or service by trade name, trademark, manufacturer, or otherwise does not necessarily constitute or imply its endorsement, recommendation, or favoring by the United States Government or any agency thereof. The views and opinions of authors expressed herein do not necessarily state or reflect those of the United States Government or any agency thereof.